Quantum many-body scars in spin-1 Kitaev chain with uniaxial single-ion anisotropy

Wen-Yi Zhang,[1,2] Ya-Nan Wang,[1,2] Dongchang Liu,[3] Jie Ren,[4] Jia Li,[5,2] Ning Wu,[6,*] Andrzej M. Oleś,[7,8,†] and Wen-Long You[1,2,‡]

[1]*College of Physics, Nanjing University of Aeronautics and Astronautics, Nanjing 211106, China*
[2]*Key Laboratory of Aerospace Information Materials and Physics (NUAA), MIIT, Nanjing 211106, China*
[3]*Mathematical Sciences Institute, The Australian National University, Canberra ACT 2601, Australia*
[4]*Department of Physics, Changshu Institute of Technology, Changshu 215500, China*
[5]*College of Engineering Physics, Shenzhen Technology University, Shenzhen 518118, China*
[6]*Center for Quantum Technology Research, School of Physics, Beijing Institute of Technology, Beijing 100081, China*
[7]*Max Planck Institute for Solid State Research, Heisenbergstrasse 1, D-70569 Stuttgart, Germany*
[8]*Institute of Theoretical Physics, Jagiellonian University, Prof. Stanisława Łojasiewicza 11, PL-30348 Kraków, Poland*

(Received 31 May 2023; revised 31 July 2023; accepted 17 August 2023; published 13 September 2023)

To establish a solid-state-based framework for the coexistence of quantum many-body scars and quantum criticality, we investigate the spin-1 Kitaev chain with uniaxial single-ion anisotropy (SIA). In the subspace with uniform $\mathbb{Z}_2$ gauge fields, this model can be exactly mapped to the spin-1/2 effective detuned PXP Hamiltonian, where the SIA plays a role of the static detuning term. The quench dynamics starting from the product states is symmetric between positive and negative values of the SIA, while a quantum phase transition from the Kitaev spin liquid to the dimer phase only occurs at the critical point with a negative D_c, implying the spontaneous breaking of the translational symmetry. We find that the coherent oscillations of quantum fidelity and certain local observables are sustained against small SIA perturbations in a quantum quench from special initial states. While the oscillation amplitudes of these observables decay with time as the SIA strength is increased, the system completely thermalizes upon approaching the critical point. In contrast, the initial polarized state, which shows an absence of revivals of quantum fidelity, will exhibit long revivals for $D < D_c$. Finally, we investigate the evolution of phase boundaries of the Kitaev spin liquid and dimer phase by introducing Heisenberg interactions, which spoil the $\mathbb{Z}_2$ gauge fields. A complete phase diagram is given by the infinite time-evolving block decimation method and the ground-state properties of each phase are accurately captured by various spin correlations. Our paper opens the door to understanding exotic connections between many-body scars and quantum criticality in systems with higher spins.

DOI: 10.1103/PhysRevB.108.104411

I. INTRODUCTION

In the past decade, there has been significant progress in understanding out-of-equilibrium dynamics of isolated quantum systems [1]. The eigenstate thermalization hypothesis (ETH) [2–7] has been regarded as a cornerstone of contemporary statistical mechanics, which states that in a thermalizing system, the expectation value of a generic local observable in individual eigenstates should be equivalent to its microcanonical average. Despite the significant success of ETH in explaining thermalization of chaotic systems, instances of ergodicity breaking are continually being discovered. The integrable systems [8–13] and many-body localization [14–20] are the most noteworthy exceptions. The strong ergodicity breaking phenomena in counterexamples, where most of the eigenstates violate the ETH, can be ascribed to the presence of conserved quantities [21]. In an integrable system, the number of conserved quantities is equal to the number of degrees of freedom [22]. On the other hand, many-body localization occurring in systems where disorder and interactions prevent the system from thermalizing can also be described by the emergence of an extensive set of quasilocal integrals of motions [23]. Recently, a Rydberg-atom quantum simulator [24] revealed the emergence of another type of ETH-violating eigenstates in certain nonintegrable quantum many-body systems, dubbed quantum many-body scar (QMBS) states [25–35]. Some specific low-entanglement states in a many-body quantum system are exceptional in that they violate the ETH and can retain quantum coherence for long times, even when the system is chaotic and thermalizing [36].

To be specific, the number of QMBSs is exponentially smaller than the Hilbert space dimension. The discovery of QMBSs has opened a paradigm for studying unusual

*wunwyz@gmail.com
†a.m.oles@fkf.mpi.de
‡wlyou@nuaa.edu.cn

Published by the American Physical Society under the terms of the Creative Commons Attribution 4.0 International license. Further distribution of this work must maintain attribution to the author(s) and the published article's title, journal citation, and DOI. Open access publication funded by the Max Planck Society.

nonequilibrium phenomena including many-body revivals and nonthermal stationary states [37,38]. Soon after, the scarred states were observed in a variety of physical systems, including *inter alia,* interacting spin chains [39,40], cold atom systems [41–43], superconducting qubits [44,45], etc. In parallel with exciting experimental advances, theoretical studies have shown that QMBSs are not related to the usual symmetries [46]. Known systems that host QMBS states also include the Affleck-Kennedy-Lieb-Tasaki model [47,48], the spin-1 XY model [49], and the generalized Fermi-Hubbard model [50]. The associated weak ergodicity breaking not only challenges the validity of ETH but also poses a different scenario of nonthermal dynamics.

Later, it was pointed out theoretically that the Rydberg experiment can be described by the one-dimensional (1D) chain of spin-1/2 degrees of freedom [51–56], where the spin-up state $|1\rangle$ corresponds to a Rydberg atom occupying an excited state and the spin-down state $|0\rangle$ denotes an atom in the ground state. Such a spin-1/2 spin chain, known as the PXP Hamiltonian and resulting from the first-order Schrieffer-Wolff transformation applied to a tilted Ising chain, is described by

$$\hat{H}_{\mathrm{PXP}} = \sum_{i=1}^{N} P_{i-1} X_i P_{i+1}, \tag{1}$$

where N is the number of sites, $X = |0\rangle\langle 1| + |1\rangle\langle 0|$ and $P = |0\rangle\langle 0|$ is the projector onto the ground state, ensuring that the nearby atoms are not simultaneously in the excited state.

Such a Rydberg blockade-induced kinetic constraint is responsible for the atypical dynamics of QMBS states. When the system is initialized at time $t = 0$ in the product state $|\psi(0)\rangle \equiv |\mathbb{Z}_k\rangle$ $(k = 1, 2, 3, 4)$, namely,

$$\begin{aligned} |\mathbb{Z}_1\rangle &= |0000\cdots00\rangle, \quad |\mathbb{Z}_2\rangle = |010101\cdots01\rangle, \\ |\mathbb{Z}_3\rangle &= |001001\cdots001\rangle, \quad |\mathbb{Z}_4\rangle = |00010001\cdots0001\rangle, \end{aligned} \tag{2}$$

the system then follows the evolution governed by the PXP Hamiltonian, $|\psi(t)\rangle = \exp(-i\hat{H}_{\mathrm{PXP}}t)|\psi(0)\rangle$. It was noted that the quantum quench from either $|\mathbb{Z}_2\rangle$ or $|\mathbb{Z}_3\rangle$ exhibits periodic revivals in the quantum fidelity,

$$F(t) = |\langle\psi(0)|\psi(t)\rangle|^2, \tag{3}$$

while $|\mathbb{Z}_1\rangle$ or $|\mathbb{Z}_4\rangle$ thermalize under time evolution. The observed oscillations and apparent nonergodic dynamics are due to the existence of equal spacing of the QMBS eigenstates [57].

Considering the experimental realization and the important role of the emergence of QMBS in the PXP model, the intensive study of the PXP model has been the subject of a separate thread of investigation of much current interest [58–62]. In fact, this effective model has a long history dating at least as far back as an effective Hamiltonian for the tilted Bose-Hubbard model [63]. The PXP model has been studied in various other contexts, including Fibonacci anyon chains [64–66], Ising models on dimer ladders [67,68], $U(1)$ lattice gauge theory in its quantum link [69–72], dipole-conserving Hamiltonians [73], the quantum Hall effect on a thin torus at filling $\nu = 1/3$ [74], etc. Meanwhile, the PXP model was extended to Floquet Hamiltonians [75], higher spins [76], and higher dimensions [77]. The PXP model can be deduced from the biaxial Ising model with both transverse and longitudinal fields at zero detuning [78] and the Bose-Hubbard model at resonance [79]. It was also claimed that there is an intimate relation between QMBS and quantum criticality [80] or quantum integrability [81].

Remarkably, the 1D PXP chain is shown to be embedded in the spin-1 Kitaev model [82,83], highlighting a solid-state-based realization of the PXP model. The celebrated Kitaev model is renowned as a prototype model of quantum spin liquid (QSL), which hosts massive long-range entanglement and fractional quasiparticles from localized spins described by bosonic/fermionic spinons and $\mathbb{Z}_2$ gauge fields [84]. Solid-state material realizations of the bond-dependent Kitaev interactions with $S = 1/2$ local moments have vitalized the research in QSLs [85,86], where strong spin-orbit coupling in a strongly correlated Mott insulator plays an essential role. $4d$ and $5d$ transition-metal compounds are proposed to be candidate materials, such as the triangular lattice $YbMgGaO_4$ [87], 1T-$TaSe_2$ [88], and $NaYbS_2$ [89]; kagome lattice $ZnCu_3(OH)_6Cl_2$ [90] and $Na_4Ir_3O_8$ [91]; honeycomb lattice α-$RuCl_3$ [92], $H_3LiIr_2O_6$ [93], Cu_2IrO_3 [94], $RuBr_3$ [95], and $BaCo_2(AsO_4)_2$ [96]; pyrochlore lattice $Ce_2Zr_2O_7$ [97] and $Ba_3Yb_2Zn_5O_{11}$ [98]. After the groundbreaking proposal for realizing the higher-spin analogs of the Kitaev interactions [99], a number of materials with strong Hund's coupling among two electrons in e_g orbitals of transition metal ions and strong spin-orbit coupling of anions have emerged as potential candidates for the $S = 1$ Kitaev model. Recently the importance of studying the higher-spin Kitaev physics has attracted a lot of attention.

Both experimental and numerical analyses have been indispensably carried out to explore the higher-spin Kitaev physics, such as $S = 1$ [100–105], $S = 3/2$ [106–108], and even $S = 2$ systems [109]. It is noteworthy that non-Kitaev interactions widely exist in candidate materials, which is a chief obstacle of keeping the system away from the pure Kitaev limit. The ferromagnetic Heisenberg interactions are generated from superexchange paths together with Kitaev interactions, in parallel with the antiferromagnetic Heisenberg term from direct-exchange paths.

For Mott insulators with two or more atoms per site, the direct on-site interactions can give rise to a nonlinear term $\propto D\sum_j (S_j^z)^2$ for $S \geqslant 1$, where D is the so-called uniaxial single-ion anisotropy (SIA) constant. Recently, theoretical [110–112] and experimental [113] studies on the Kitaev model with additional SIA have attracted increasing attention. In this paper, we will show that the static detuning in the PXP model, which describes the static frequency difference between the ground and excited states, can be mimicked by the additional SIA in the spin-1 Kitaev model, which normally stems from zero-field splitting due to a crystal-field anisotropy. Upon varying the strength of the SIA, a corresponding second-order phase transition will occur with a translational symmetry breaking. A comprehensive study of the phase diagram has been conducted by incorporating significant Heisenberg interactions. In the numerical calculation, we employ the exact diagonalization (ED) method, the time-evolving a matrix product state (MPS) with matrix product operators (MPOs) [114] based on ITensor [115]

and the infinite time-evolving block decimation (iTEBD) algorithm [116].

The remainder of this paper is organized as follows: In Sec. II, we present the spin-1 Kitaev model with SIA (the KD model) and deduce the effective spin-1/2 detuned PXP model in the ground-state manifold. The QMBSs in the spin-1 KD model are studied in detail. In Sec. III, we investigate the quantum criticality in the KD model and find the characteristics of the dimer phase. Under the cooperative effects of the SIA and Heisenberg interactions (the KHD model), we reveal the rich quantum phase diagram of KHD model in Sec. IV. The summary and conclusion are given in Sec. V.

II. SPIN-1 KITAEV CHAIN WITH UNIAXIAL SINGLE-ION ANISOTROPY

In this paper, we consider a spin-1 Hamiltonian composed of the Kitaev interaction and SIA, given by

$$\hat{H}_{\rm KD} = \sum_{j=1}^{N/2} \left(K_{2j-1} S^x_{2j-1} S^x_{2j} + K_{2j} S^y_{2j} S^y_{2j+1}\right) + \sum_{j=1}^{N} D_j \left(S^z_j\right)^2, \tag{4}$$

where K_j parameterizes the strength of the bond-dependent Kitaev exchange coupling between two neighboring sites $\langle j, j{+}1\rangle$, and D_j denotes the amplitude of the SIA at the jth site. S^a_j $(a = x, y, z)$ is the a component of the spin-1 operator at the jth site among total N sites, obeying the SU(2) algebra, i.e., $[S^a_i, S^b_j] = i\delta_{ij}\epsilon_{abc} S^c_j$, with the antisymmetric tensor ϵ_{abc} and $(\boldsymbol{S}_j)^2 = S(S+1) = 2$.

We will work with a special spin-1 representation, i.e.,

$$|x\rangle = \frac{1}{\sqrt{2}}(|{-}1\rangle - |1\rangle), \quad |y\rangle = \frac{i}{\sqrt{2}}(|{-}1\rangle + |1\rangle),$$
$$|z\rangle = |0\rangle, \tag{5}$$

where $|m\rangle$ is the eigenstate of the spin operator S^z with eigenvalues $m = -1, 0, 1$. In such a representation, we have $S^a_{bc} = -i\epsilon_{abc}$, and $\{S^x, S^y, S^z\}$ are given by

$$\begin{pmatrix} 0 & 0 & 0 \\ 0 & 0 & -i \\ 0 & i & 0 \end{pmatrix}, \begin{pmatrix} 0 & 0 & i \\ 0 & 0 & 0 \\ -i & 0 & 0 \end{pmatrix}, \begin{pmatrix} 0 & -i & 0 \\ i & 0 & 0 \\ 0 & 0 & 0 \end{pmatrix}. \tag{6}$$

The corresponding site parity matrices are defined as $\Sigma^a_j \equiv e^{i\pi S^a_j} = 1 - 2(S^a_j)^2$ and become diagonal:

$$\begin{pmatrix} 1 & 0 & 0 \\ 0 & -1 & 0 \\ 0 & 0 & -1 \end{pmatrix}, \begin{pmatrix} -1 & 0 & 0 \\ 0 & 1 & 0 \\ 0 & 0 & -1 \end{pmatrix}, \begin{pmatrix} -1 & 0 & 0 \\ 0 & -1 & 0 \\ 0 & 0 & 1 \end{pmatrix}. \tag{7}$$

It has been revealed that different Ising interactions on odd and even bonds in Eq. (4) can be rewritten into a similar form through a unitary transformation on the even sites [83,117],

$$U = \prod_j \exp\left(i\pi S^x_{2j}\right) \exp\left(i\frac{\pi}{2} S^z_{2j}\right), \tag{8}$$

which gives $US^x_{2j}U^\dagger = S^y_{2j}$, $US^y_{2j}U^\dagger = S^x_{2j}$, and $US^z_{2j}U^\dagger = -S^z_{2j}$, as well as $U|x\rangle = |y\rangle$, $U|y\rangle = |x\rangle$, $U|z\rangle = -|z\rangle$. Note that the order of rotations about x and z axes in Eq. (8) is essential as they do not commute. After the unitary transformation, the Kitaev exchange couplings in Eq. (4) take a translation-invariant form:

$$\tilde{H}_{\rm K} = \sum_{j=1}^{N} K_j S^x_j S^y_{j+1}. \tag{9}$$

It is easy to see that the SIA term remains in its original form and the Hamiltonian Eq. (4) can be rewritten:

$$\tilde{H}_{\rm KD} = \sum_{j=1}^{N} K_j S^x_j S^y_{j+1} + D_j \left(S^z_j\right)^2. \tag{10}$$

Note that the sign of the Kitaev interactions is still under debate with conflicting results from theoretical and experimental studies [118,119]. Hereafter, the uniform couplings with $K_j = 1$ and $D_j = D$ $(\forall j)$ are assumed unless otherwise specified.

Under the rotation Eq. (8), the local bond parity operators are defined by

$$\hat{W}_j = \Sigma^y_j \, \Sigma^x_{j+1}. \tag{11}$$

One can readily find that $\hat{W}_j$ is invariant by inspecting $[\hat{W}_j, \tilde{H}_{\rm KD}] = 0$. As the eigenvalues of Σ^a_j in Eqs. (7) are ± 1, the eigenvalues of $\hat{W}_j$ are related to $\mathbb{Z}_2$-valued invariants, i.e., $w_j = \pm 1$. It is straightforward to deduce from Eq. (7) that for a pair of nearest-neighbor sites $\langle j, j{+}1\rangle$, total $3{\times}3 = 9$ allowed states can be distinguished into the $w_j = 1$ sector spanned by $|xy\rangle$, $|xz\rangle$, $|yx\rangle$, $|zy\rangle$, $|zz\rangle$, and the $w_j = -1$ sector spanned by $|xx\rangle$, $|yy\rangle$, $|yz\rangle$, $|zx\rangle$. Hence, the whole Hilbert space $\mathcal{H}$ can be decomposed into 2^N dynamically disconnected Krylov subspaces of unequal sizes characterized by $\vec{w} = \{w_1, w_n, \ldots, w_N\}$ as

$$\mathcal{H} = \bigoplus_{n=1}^{2^N} \mathcal{K}_n. \tag{12}$$

The Krylov subspace $\mathcal{K}_n$ is spanned by

$$\{\mathcal{K}_n\} \equiv \text{Span}\left\{|\psi_n\rangle, \tilde{H}_{\rm KD}|\psi_n\rangle, \tilde{H}^2_{\rm KD}|\psi_n\rangle, \cdots\right\}, \tag{13}$$

where $|\psi_n\rangle$ is the so-called root state, which is a product state having explicit $\mathbb{Z}_2$ symmetries.

We have identified the ground state of the spin-1 Kitaev chain lies within the flux-free sector, i.e., $\vec{w} = \{1, 1, \ldots, 1\}$ [82]. In such a constrained Hilbert space, there is one-to-one mapping between base configurations $\{\tilde{\mathcal{K}}_{S=1}\}$ of Eq. (9) within the flux-free sector and the configurations $\{\mathcal{K}_{S=1/2}\}$ of Eq. (1) with nearest neighbor exclusion. The rule for constructing the mapping is simple. The one-to-one mapping between the five allowed two-site configurations for a pair of nearest-neighbor sites $\langle j, j{+}1\rangle$ and spin-1/2 degree of freedom for the bond center $j + 1/2$ is given by [120]

$$|\cdots zz\cdots\rangle_{j,j+1} \leftrightarrow |\cdots\downarrow\downarrow\downarrow\cdots\rangle_{j-\frac{1}{2},j+\frac{1}{2},j+\frac{3}{2}},$$
$$|\cdots yx\cdots\rangle_{j,j+1} \leftrightarrow |\cdots\downarrow\uparrow\downarrow\cdots\rangle_{j-\frac{1}{2},j+\frac{1}{2},j+\frac{3}{2}},$$
$$|\cdots zy\cdots\rangle_{j,j+1} \leftrightarrow |\cdots\downarrow\downarrow\uparrow\cdots\rangle_{j-\frac{1}{2},j+\frac{1}{2},j+\frac{3}{2}},$$
$$|\cdots xz\cdots\rangle_{j,j+1} \leftrightarrow |\cdots\uparrow\downarrow\downarrow\cdots\rangle_{j-\frac{1}{2},j+\frac{1}{2},j+\frac{3}{2}},$$
$$|\cdots xy\cdots\rangle_{j,j+1} \leftrightarrow |\cdots\uparrow\downarrow\uparrow\cdots\rangle_{j-\frac{1}{2},j+\frac{1}{2},j+\frac{3}{2}}. \tag{14}$$

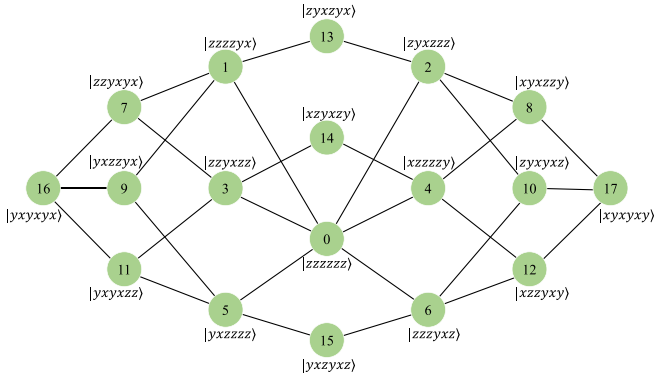

FIG. 1. The Hilbert space graph of the Kitaev Hamiltonian in Eq. (9) within the $\vec{w}$={1, 1, 1, 1, 1, 1} subspace for $N = 6$ sites with periodic boundary conditions. The nodes of the graph $|m\rangle$ ($m = 0, 1, 2, \ldots, 17$) label the allowed product states, and the edges connect product state configurations that differ by an excitation $|\cdots zz\cdots\rangle \leftrightarrow |\cdots yx\cdots\rangle$ due to the action of the Hamiltonian.

It is worth noting that the prime lattice of the spin-1 Kitaev chain is defined on sites $\{j\}$, while the dual lattice of the spin-1/2 PXP model lives on the linking bonds at sites $\{j + 1/2\}$. This mapping from sites to bonds includes links to the two surrounding sites and vice versa, which becomes subtle for open boundary conditions. As an example, the four product states given by Eqs. (2) can be mapped to the following states in $\{\tilde{\mathcal{K}}_{S=1}\}$:

$$|\widetilde{\mathbb{Z}}_1\rangle = |zzzz\cdots zz\rangle, \quad |\widetilde{\mathbb{Z}}_2\rangle = |xyxyxy\cdots xy\rangle,$$
$$|\widetilde{\mathbb{Z}}_3\rangle = |yxzyxz\cdots yxz\rangle, \quad |\widetilde{\mathbb{Z}}_4\rangle = |yxzzyxzz\cdots yxzz\rangle. \quad (15)$$

The simplest root configuration in $\{\tilde{\mathcal{K}}_{S=1}\}$ is the product state $|\widetilde{\mathbb{Z}}_1\rangle$, which is the ground state in the $D \to \infty$ limit, and the Hilbert space of this sector can be constructed by successively applying the Hamiltonian on this root state, i.e.:

$$\{\tilde{\mathcal{K}}_{S=1}\} \equiv \text{Span}\big\{|\widetilde{\mathbb{Z}}_1\rangle, \tilde{H}_{\text{K}}|\widetilde{\mathbb{Z}}_1\rangle, \tilde{H}_{\text{K}}^2|\widetilde{\mathbb{Z}}_1\rangle, \cdots\big\}. \quad (16)$$

The corresponding dimension d of the flux-free sector is proven to be a Lucas number [83], i.e., $d = F_{N-1} + F_{N+1}$, where F_ℓ is the ℓth Fibonacci number. More precisely, $d = g^N + g^{-N}$, with $g = (1 + \sqrt{5})/2$ being the golden ratio. This exponentially large subspace belongs to the largest Krylov subspace among the exponential number of Krylov subspaces, implying strong fragmentation of the Hilbert space. The graphical representation of the constrained Hilbert space in the $\vec{w}$={1, 1, . . . , 1} subspace is schematically shown in Fig. 1 for $N = 6$. The vertices in the 18-dimensional hypercube are uniquely labeled by the connected configurations Eqs. (16), which have been arranged by the action of the Kitaev Hamiltonian $\tilde{H}_{\text{K}}$ on the product state $|\cdots zzzz\cdots\rangle$.

The process of bond converting $|\cdots zz\cdots\rangle_{j,j+1} \leftrightarrow |\cdots yx\cdots\rangle_{j,j+1}$ under the action of $\tilde{H}_K$ corresponds to the spin flip $|\cdots 0\cdots\rangle_{j+1/2} \leftrightarrow |\cdots 1\cdots\rangle_{j+1/2}$ in $\{\mathcal{K}_{S=1/2}\}$. In this regard, the spin-1 Kitaev chain with periodic boundary conditions can be exactly mapped to the a single qubit-flip model represented by the effective spin-1/2 PXP model in Eq. (1). Remarkably, we find the ground state remains in the flux-free sector even in the presence of the SIA. The action of

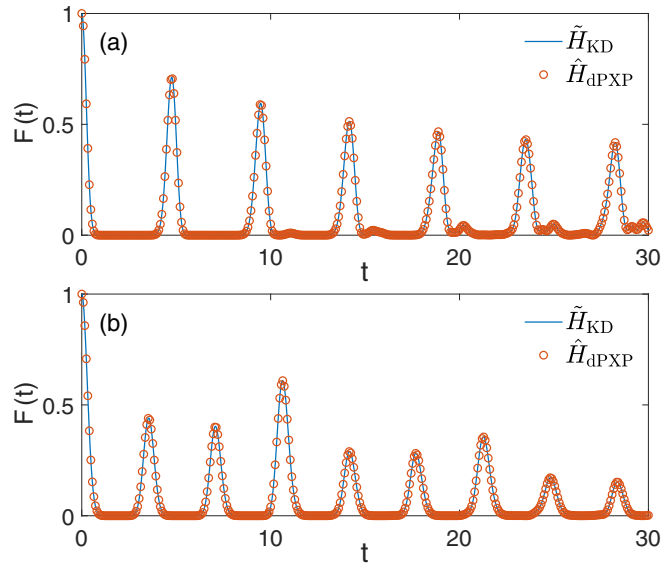

FIG. 2. Characteristic quantum features of the spin-1 KD model and the spin-1/2 detuned PXP model with $D = 0.1$. Quantum fidelity $F(t)$ for $\tilde{H}_{\text{KD}}$ in Eq. (10) [$\hat{H}_{\text{dPXP}}$ in Eq. (18)] starting from the initial states: (a) $|\widetilde{\mathbb{Z}}_2\rangle$ ($|\mathbb{Z}_2\rangle$) with $N = 18$ and (b) $|\widetilde{\mathbb{Z}}_3\rangle$ ($|\mathbb{Z}_3\rangle$) with $N = 18$.

the SIA term on the active bases yields

$$D\big[\big(S_j^z\big)^2 + \big(S_{j+1}^z\big)^2\big]|\cdots yx\cdots\rangle_{j,j+1} = 2D|\cdots yx\cdots\rangle_{j,j+1},$$
$$D\big[\big(S_j^z\big)^2 + \big(S_{j+1}^z\big)^2\big]|\cdots zz\cdots\rangle_{j,j+1} = 0, \quad (17)$$

which results in an effective detuning term on the spin-1/2 degrees of freedom, such that the effective Hamiltonian can be mapped to the spin-1/2 detuned PXP model,

$$\hat{H}_{\text{dPXP}} = \sum_{i=1}^{N} P_{i-1}X_iP_{i+1} + 2D\sum_{i=1}^{N} P_{i-1}n_iP_{i+1}, \quad (18)$$

where $n = 1 - P = |1\rangle\langle 1|$. Note that in both Eqs. (1) and (18), i labels the bonds between sites, while the index j labels the sites in Eq. (10). The detailed derivation of Eq. (18) can be found in Appendix A.

The detuning term is commonly prevalent in practical experiments. The static detuning (also called chemical potential [121]) of the driving laser from the excited state can be finely tuned in cold-atom platforms. It has been noted that quantum quench from initial states $|\widetilde{\mathbb{Z}}_2\rangle$ or $|\widetilde{\mathbb{Z}}_3\rangle$ results in coherent oscillations, indicating the existence of ETH-violating QMBSs. In our ED simulation [122], the time-evolved operator $\exp(-i\hat{H}t)$ governed by either $\tilde{H}_{\text{KD}}$ as defined in Eq. (10) or $\hat{H}_{\text{dPXP}}$ as given in Eq. (18) is discretized using time steps of $dt = 0.01$, and the time-evolved state $|\psi(t)\rangle$ is subsequently computed using the fourth-order Runge-Kutta method within the corresponding constraint Hilbert space. Figure 2 demonstrates these oscillations in the dynamics of the quantum fidelity for $D = 0.1$. The periodic revivals for the spin-1 KD model Eq. (10) starting from the $|\widetilde{\mathbb{Z}}_2\rangle$, $|\widetilde{\mathbb{Z}}_3\rangle$ initial states completely coincide with the ones observed for the spin-1/2 detuned PXP model, which starts from the corresponding $|\mathbb{Z}_2\rangle$, $|\mathbb{Z}_3\rangle$ initial states.

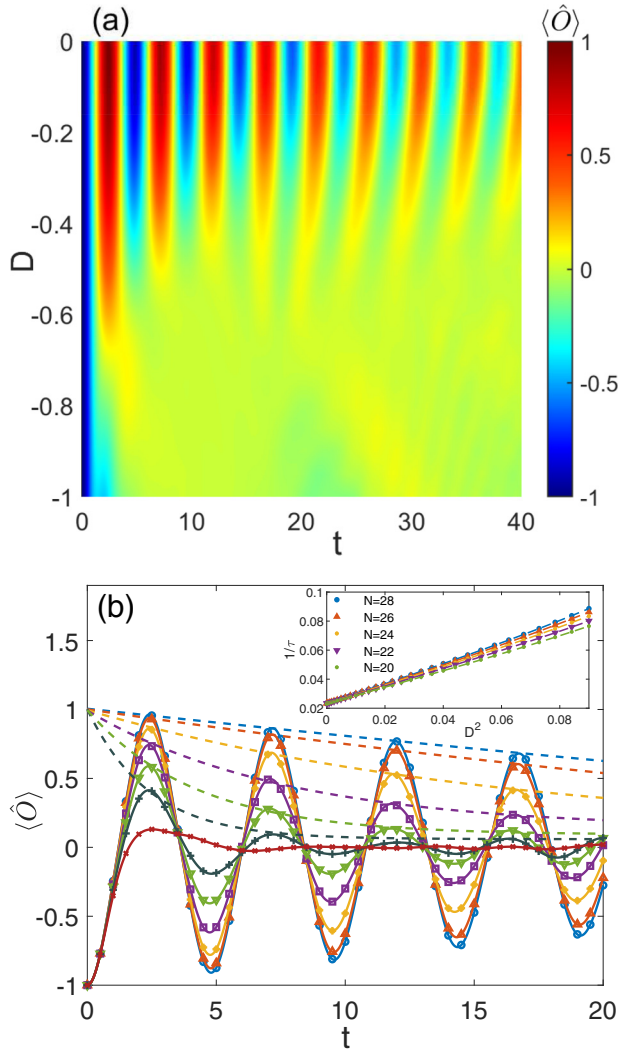

FIG. 3. (a) The contour map of time evolution of $\langle\hat{O}\rangle$ defined in Eq. (19) of $\tilde{H}_{\mathrm{KD}}$ Eq. (10) in a system of $N = 28$ spins prepared in $|\widetilde{\mathbb{Z}}_2\rangle$ obtained by ED. (b) The time evolution of $\langle\hat{O}\rangle$ for different values of D. The curves correspond to $D = 0.0$, -0.1, -0.2, -0.3, -0.4, -0.5, -0.655 (from bottom to top at $t = 5$). The dashed lines are fits capturing the amplitude decay. Inset shows inverse lifetime of $\langle\hat{O}(t)\rangle$ envelop with increasing D^2. We extract the decay time by fitting the data to the scaling ansatz $\langle\hat{O}(t)\rangle = Ae^{-t/\tau}\cos\omega t$ (see main text).

Recent studies have signified an intimate relation between QMBS and quantum criticality [80,81]. As D is tuned to $D_c \approx -0.655$, the ground state of the detuned PXP model undergoes an Ising phase transition associated with a spontaneous breaking of $\mathbb{Z}_2$ symmetry [123–126]. The nonthermalizing dynamics can also be captured by measuring the expectation values of certain local observables [127], e.g.:

$$\langle\hat{O}\rangle = \tfrac{1}{2}\langle[(S_1^+)^2 + (S_1^-)^2]\rangle. \tag{19}$$

Under the dual transformation Eqs. (14), the correlator $\langle\hat{O}\rangle$ of the KD model in Eq. (10) is found to be equivalent to the density imbalance, $\langle n_2\rangle - \langle n_1\rangle$, an observable corresponding to the staggered magnetization in the detuned PXP model in Eq. (18). Performing a quantum quench from an initial state

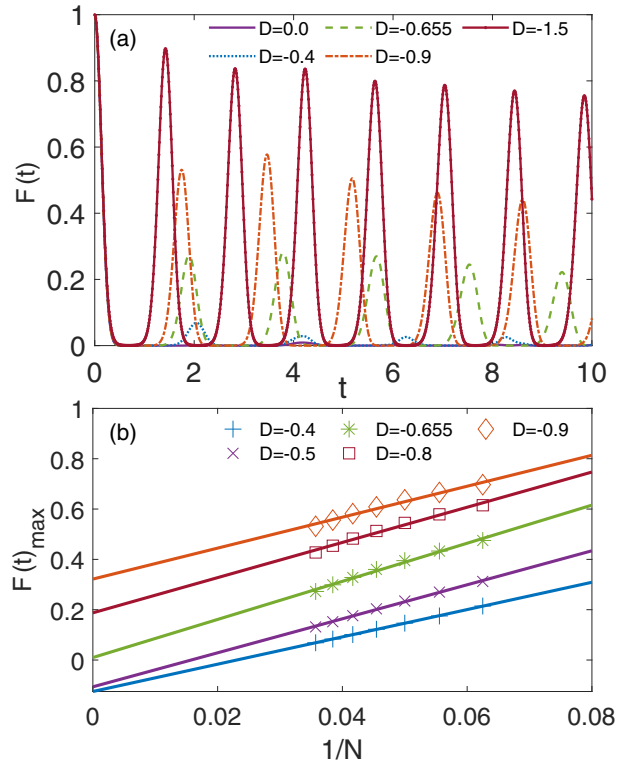

FIG. 4. The dynamic evolution of the spin-1/2 detuned PXP model starting from the initial state $|\mathbb{Z}_1\rangle$: (a) The quantum fidelity $F(t)$ with respect to different D for $N = 28$. (b) Finite-size scaling of $F(t)$ for the first peak in (a).

$|\widetilde{\mathbb{Z}}_2\rangle$ leads to nearly perfect coherent dynamics. The coherence oscillations persist for long times for $D = 0$, as shown in Fig. 3. Note that the values of $F(t)$ and $\langle\hat{O}\rangle$ are independent of the sign of D when the system starts from the product states, $|\widetilde{\mathbb{Z}}_k\rangle$ (see details in Appendix B).

As exhibited in Fig. 3(a), these oscillations are found to be remarkably robust to small SIA perturbations, while moderate perturbations make the oscillations dampen sharply until D reaches a threshold value. One carefully observes from Fig. 3(b) that the oscillations remain strong for deviations up to $D \approx \pm D_c$, and there is barely oscillation at $D = D_c$, upon which the thermalization completely sets in. Suppose that the envelope of $\langle\hat{O}\rangle$ can be described by exponentially decaying oscillations, $\langle\hat{O}(t)\rangle = Ae^{-t/\tau}\cos\omega t$ over time t, with the fitting parameters A, τ, and ω. We observe that the inverse lifetime approximately follows $\tau^{-1} \sim D^2$ at small D, reminiscent of Fermi's golden rule [128]. Additionally, it is worth noting that the decay rate of oscillations τ^{-1} at $D = 0$ remains small but finite, suggesting that the $|\widetilde{\mathbb{Z}}_2\rangle$ initial state only approximates the near-perfect scar states in the standard PXP model. The fact that the quantum critical point D_c is negative and there is no quantum phase transition for positive D, combined with the significant difference between the ground states as D tends to infinity, undermine the viewpoint that QMBSs and quantum criticality are directly bridged.

For $D = 0$, the quantum fidelity revivals do not occur for the initial state $|\mathbb{Z}_1\rangle$. As D decreases from zero, surprisingly, there will be a slight revival in fidelity for the same initial

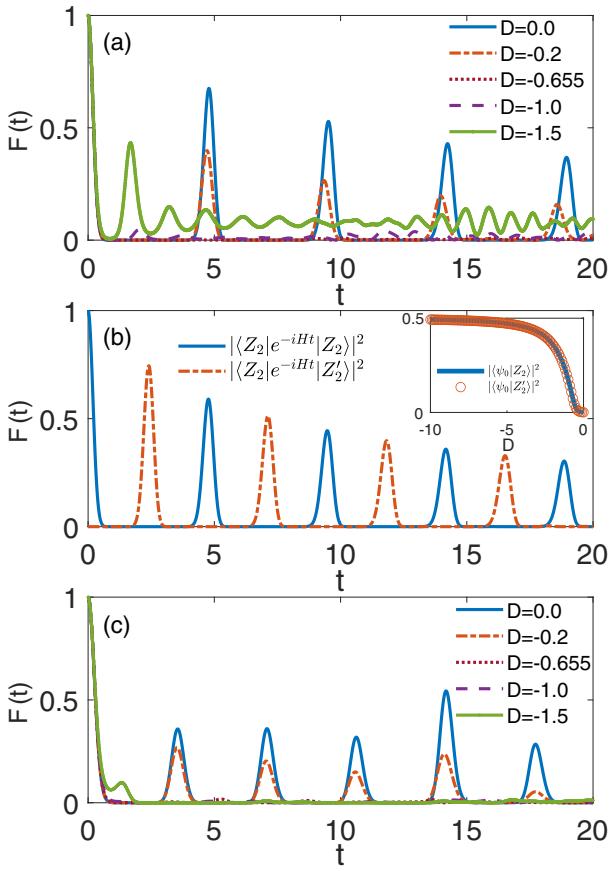

FIG. 5. Dynamics of quantum fidelity for the detuned PXP model: (a) Starting from initial state $|\mathbb{Z}_2\rangle$ for $N = 28$ sites; (b) the overlaps between the product state $|\mathbb{Z}_2\rangle$ and the time-evolved state starting from $|\mathbb{Z}_2\rangle$ (solid) and $|\mathbb{Z}_2'\rangle$ (dashed) with $D = -0.1$ for $N = 28$ sites. The inset shows the overlap of the prequench ground state with $|\mathbb{Z}_2\rangle$ and $|\mathbb{Z}_2'\rangle$. (c) Starting from initial $|\mathbb{Z}_3\rangle$ state for $N = 24$ sites.

state. As D continues to decrease, the oscillation becomes more clearly visible with smaller periods, as observed in Fig. 4(a). When the value of D is smaller than the critical value D_c, the revivals become more pronounced. Finite-size scaling in Fig. 4(b) reveals that the first peak will disappear for large N before the value of D exceeds D_c. When $D > D_c$, the intercepts of the finite-size scaling curves become negative, which is an unphysical artifact and indicates that the linear fit is no longer applicable. In contrast, the first peak will always have a finite value for $D < D_c$ in the thermodynamic limit, which may be related to asymptotic scars [129].

Figure 5(a) shows the quantum fidelity of $\hat{H}_{\mathrm{dPXP}}$ with different values of D for $N = 28$ using the initial $|\mathbb{Z}_2\rangle$ state. Remarkably, when D decreases from zero, persistent oscillations first decrease when $D > D_c$, then dampen in the critical regime $D \approx D_c$, and finally revive beyond the critical point for $D < D_c$. Figure 5(b) shows the overlaps between the $|\mathbb{Z}_2\rangle$ state and the time-evolved state starting from $|\mathbb{Z}_2\rangle$ and $|\mathbb{Z}_2'\rangle$, where $|\mathbb{Z}_2'\rangle \equiv |101010\cdots10\rangle$ is obtained by translating one lattice spacing on $|\mathbb{Z}_2\rangle$.

The peaks of the oscillations of $|\langle\mathbb{Z}_2|\exp(-i\hat{H}t)|\mathbb{Z}_2\rangle|^2$ and $|\langle\mathbb{Z}_2|\exp(-i\hat{H}t)|\mathbb{Z}_2'\rangle|^2$ are separated by half a period. We also show the fidelity between the $|\mathbb{Z}_2\rangle$ state and the ground state $|\psi_0\rangle$ at different values of D, as shown in the inset of Fig. 5(b). We observe that as D approaches negative infinity, the fidelity between the ground state and $|\mathbb{Z}_2\rangle$ ($|\mathbb{Z}_2'\rangle$) gradually approaches $1/2$. We remark that due to the Hilbert space constraint, at most, half of the atoms could be in the spin-up states. In fact, in the limit of $D \to -\infty$, the ground state becomes an antiferromagnetic phase in the zero-momentum sector, i.e., $|\psi_0(D = -\infty)\rangle = (|\mathbb{Z}_2\rangle + |\mathbb{Z}_2'\rangle)/\sqrt{2}$. In contrast, Fig. 5(c) demonstrates a complete absence of revivals for $D < D_c$ in the case of an initial state of $|\mathbb{Z}_3\rangle$, featuring approximate QMBS states vanish.

We next investigate the dynamics of bipartite entanglement entropies in both the KD model and the detuned PXP model. We choose region A to be one-half of the chain and compare the dynamics of half-chain entanglement entropy $\mathcal{S}$ in a quantum quench from different initial states for both the spin-1 KD model and the spin-1/2 detuned PXP model with periodic boundary conditions. In our numerical calculation for the $S = 1$ KD model [cf., Figs. 6(a) and 6(b)], we utilize the time-evolving MPS approach with MPOs [115], where the bond dimension is set as $\chi = 500$ and the time step is $dt = 0.025$. The bipartite entanglement of the evolved state starting from the initial state $|\widetilde{\mathbb{Z}}_2\rangle$ is shown in Fig. 6(a). When D is small negative, $\mathcal{S}$ increases slowly over time while exhibiting coherent oscillations, featuring the many-body revivals. As D becomes more negative, the temporal growth rate of the bipartite entanglement increases and the coherent oscillation becomes weak. When D approaches D_c, the entanglement $\mathcal{S}$ almost increases linearly with time until saturation and the coherent oscillations disappear, implying that the system quickly thermalizes.

When D is smaller than D_c, the linear growth rate of entanglement decreases with a smaller saturated value of entanglement. We find that the growth of entanglement entropy starting from the initial state $|\widetilde{\mathbb{Z}}_3\rangle$ exhibits a similar trend, as shown in Fig. 6(b). For comparison, we show the evolution of the bipartite von Neumann entanglement entropy of the spin-1/2 detuned PXP model when the system is initially prepared in the state $|\mathbb{Z}_2\rangle$ ($|\mathbb{Z}_3\rangle$) in Fig. 6(c) [6(d)]. One observes $\mathcal{S}$ is gradually growing for D being small negative, while undergoing an extremely fast growth until saturation at $D \approx D_c$. When $D < D_c$, the growth of entanglement entropy slows down again. Although the two Hamiltonians and their corresponding initial states are unitarily equivalent under the local transformation Eqs. (14), the entanglement evolution displays noticeable differences. Notably, the coherent oscillations for $S = 1/2$ become considerably weaker compared to those for $S = 1$ when $0 \geqslant D > D_c$. The bipartite entanglement entropy heavily depends on the choice of presentations and bipartition methods. This can be perceived by an analytical example presented in Appendix A of Ref. [83].

III. QUANTUM PHASE TRANSITION OF SPIN-1 KITAEV CHAIN WITH UNIAXIAL SINGLE-ION ANISOTROPY

In the previous section, we discovered a close relationship between QMBS states and quantum criticality. Accordingly, we proceed to investigate the quantum phase transition of the spin-1 KD model given by Eq. (4). We adopt the iTEBD

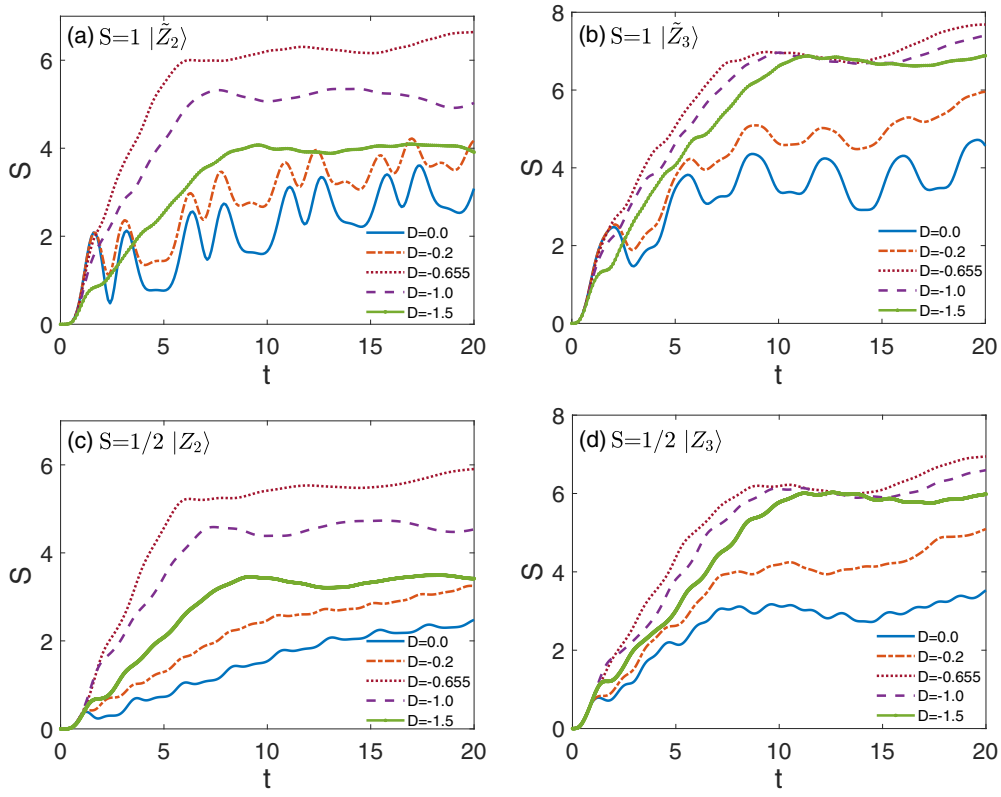

FIG. 6. Evolution of the bipartite entanglement entropy in the quantum quench from initial states: (a) $|\widetilde{\mathbb{Z}}_2\rangle$, (b) $|\widetilde{\mathbb{Z}}_3\rangle$ for the spin-1 KD model, (c) $|\mathbb{Z}_2\rangle$, and (d) $|\mathbb{Z}_3\rangle$ states for the spin-1/2 detuned PXP model with $N = 24$.

algorithm with a bond dimension of $\chi = 120$ [122]. In our calculations, we set the imaginary time as $10^{-5.5}$ to ensure a truncation error smaller than 10^{-8}. The advantage of using iTEBD is its capability to treat infinite-size systems directly, providing numerical evidence for the emergence of a symmetry-breaking phase. According to the core spirit of the Landau-Ginzburg-Wilson paradigm, the quantum phase transition of a many-body system can be described by a well-defined order parameter. We calculate the two-point correlations between the ith and jth sites,

$$C^{ab}(i,j) = \left\langle S_i^a \exp\left(i\theta \sum_{l=i+1}^{j-1} S_l^a\right) S_j^b \right\rangle, \quad a,b = x,y,z, \tag{20}$$

which can detect different symmetry-breaking phases. Equation (20) reduces to two-point correlations for $\theta = 0$, while it becomes the den Nijs-Rommelse string order parameter for $\theta = \pi$ [130,131]. Note that there is no phase accumulated for two nearest-neighboring sites and a general angle θ could capture the hidden topological orders [132]. The Hamiltonian in Eq. (4) is invariant under a joint operation that combines a $\pi/2$-rotation about the z axis and a single-site translation, which implies that on a finite-size system,

$$\begin{aligned} &C^{xx}(1,2) = C^{yy}(2,3), \quad C^{yy}(1,2) = C^{xx}(2,3), \\ &C^{zz}(1,2) = C^{zz}(2,3). \end{aligned} \tag{21}$$

The joint symmetry can be expressed in the rotated Hamiltonian Eq. (10) as $\tilde{C}^{xy}(1,2) = \tilde{C}^{xy}(2,3)$, $\tilde{C}^{yx}(1,2) = \tilde{C}^{yx}(2,3)$, and $\tilde{C}^{zz}(1,2) = \tilde{C}^{zz}(2,3)$.

In the zero-field limit, the ground state is a gapped Kitaev spin liquid (KSL), which is stable against nonzero perturbations [82]. Upon applying the uniaxial SIA D, the ground state remains in the flux-free sector, i.e., $\vec{w}=\{1,1,\ldots,1\}$. At a large positive D, the spins are confined to $|z\rangle$ (i.e., $\langle S_j^z\rangle = 0$), while for a large negative D the ground states are restricted to $|x\rangle$ or $|y\rangle$ ($\langle S_j^z\rangle = \pm 1$). Surprisingly, unlike the KSL phase, a notable difference between $C^{xx}(1,2)$ and $C^{yy}(2,3)$ or, equivalently, $\tilde{C}^{xy}(1,2)$ and $\tilde{C}^{xy}(2,3)$, implies the spontaneous breaking of the translational symmetry, in the way the system hosts the dimer order. The dimer phase is characterized by an alternation of nearest-neighbor spin-spin correlations, which is characterized by the difference of $\langle \boldsymbol{S}_i \cdot \boldsymbol{S}_j \rangle$ between the odd bonds and even bonds. A finite dimer order parameter is defined by

$$O_D = |\langle \boldsymbol{S}_{2j-1} \cdot \boldsymbol{S}_{2j}\rangle - \langle \boldsymbol{S}_{2j} \cdot \boldsymbol{S}_{2j+1}\rangle|. \tag{22}$$

To be more specific, we can also examine the x, y, and z components of the dimer order parameter, such as

$$\begin{aligned} O_D^x &= \left|\left\langle S_{2j-1}^x S_{2j}^x\right\rangle - \left\langle S_{2j}^y S_{2j+1}^y\right\rangle\right|, \\ O_D^y &= \left|\left\langle S_{2j-1}^y S_{2j}^y\right\rangle - \left\langle S_{2j}^x S_{2j+1}^x\right\rangle\right|, \\ O_D^z &= \left|\left\langle S_{2j-1}^z S_{2j}^z\right\rangle - \left\langle S_{2j}^z S_{2j+1}^z\right\rangle\right|. \end{aligned} \tag{23}$$

Note that the dimer order arises from the Kitaev interactions Eq. (4), leading to the characterization of the x and y components as the differences between distinct types of Ising interactions on odd and even bonds. Figure 7(a) illustrates that the x component of the dimer order parameter increases

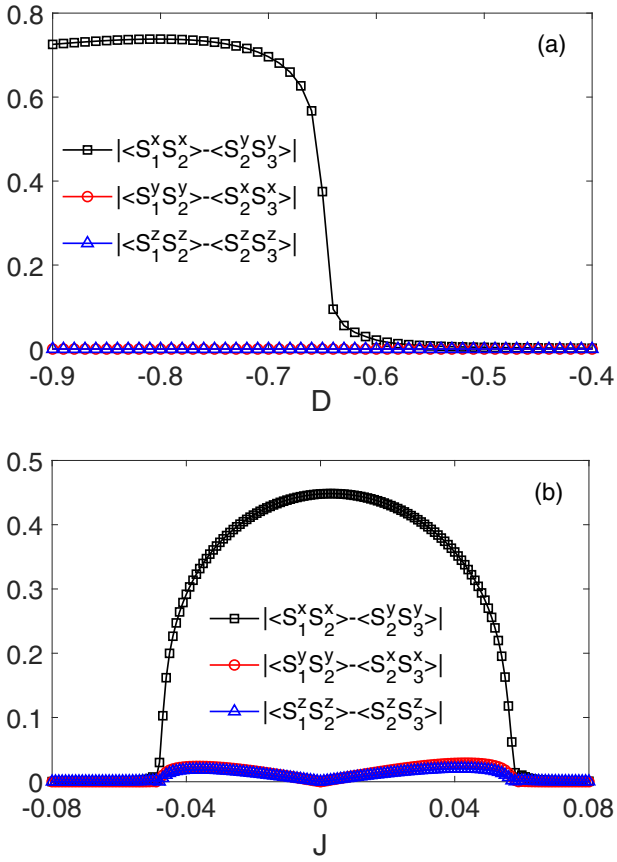

FIG. 7. The three components of dimer order parameter O_D as a function of D. (a) From the dimer phase to the KSL phase at $J = 0$. (b) From the FM_z phase to the dimer phase to the AFM_z phase at $D = -2$. Here we use the iTEBD method and the bond dimension is set as $\chi = 120$.

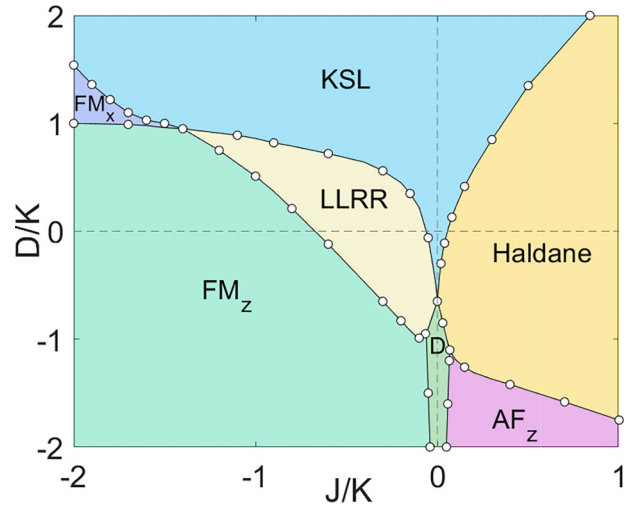

FIG. 8. Quantum phase diagram of the spin-1 Kitaev-Heisenberg model with uniaxial single-ion anisotropy calculated by the iTEBD method with bond dimension $\chi = 120$. The quantum phase transition from the dimer phase (D) to the KSL phase occurs at $D_c = -0.655$ for $J = 0$ (vertical dashed line). At $D = 0$ (horizontal dashed line), the KSL is stable in the range of $|J| < 0.08$.

smoothly from zero to a finite value as the parameter D is decreased and crosses the critical value $D_c = -0.655$, indicating a second-order transition occurs at D_c. The presence of nonvanishing dimer correlations for $D > D_c$ can be attributed to the limitations imposed by the finite bond dimension. The dimer orders are associated with the spontaneous breaking of translational symmetry of O_D^x in an infinite system. The emergence of the dimer ordering is distinct from the general mechanism for the formation of dimerized phases, which is typically induced by inherent bond alternation and the resulting breaking of translational symmetry. The ground state is two-fold degenerate for $D < D_c$ in the thermodynamic limit, which is in contrast to the gapped ground state for $D > D_c$.

IV. EFFECT OF HEISENBERG INTERACTIONS

It has been recognized the scarred states display anomalous stability in the Kitaev phase in the vicinity of $D = 0$ [83]. QSLs are widely believed to be crucially driven by the Kitaev interactions in spin-orbit-coupled materials. While Kitaev interactions are highly anisotropic, the isotropic Heisenberg interaction, ubiquitous in real materials, can also play an essential role in the emergence of exotic phenomena in many-body systems. The relevance of the Kitaev phase in a broader regime becomes paramount for understanding scar stability and its potential applications in solid-state systems. To address this point, we investigate the evolution of the phase boundaries of the KSL and the dimer phase by introducing Heisenberg interactions that disrupt the $\mathbb{Z}_2$ gauge fields, as given by

$$\hat{H}_J = J \sum_{j=1}^{N} \boldsymbol{S}_j \cdot \boldsymbol{S}_{j+1}. \tag{24}$$

When the parameters $\{D, J\}$ vary, the competitions of various correlations trigger miscellaneous phase transitions. Figure 8 depicts the phase diagram for the Kitaev-Heisenberg chain with uniaxial SIA (KHD model). The phase diagram is much richer than expected. Seven distinct phases are identified, including the KSL phase, dimer phase (D), the spin nematic phase with a left-left-right-right pattern (LLRR), Haldane phase, x-component ferromagnetic (FM_x) phase, z-component ferromagnetic (FM_z) phase, and z-component antiferromagnetic (AFM_z) phase.

The joint symmetry Eqs. (21) is preserved in the whole KSL phase for the infinite system. It has been reported that on the line of $D = 0$ (the horizontal dashed line in Fig. 8), the ground state of the Kitaev-Heisenberg model undergoes the FM_z phase, the LLRR phase, the KSL, and the Haldane phase with increasing J. The successive second-order quantum phase transitions occur at $J_c = -0.6$, -0.08, and 0.08, respectively [82]. For $J = 0$ and $D = 0$, the pure Kitaev chain hosts only two nearest-neighboring antiferromagnetic orders $\langle S_{2j-1}^x S_{2j}^x\rangle$ and $\langle S_{2j}^y S_{2j+1}^y\rangle$ while other correlations vanish, similar to the spin-1/2 Kitaev honeycomb model [133]. Away from the Kitav limit, the two-spin correlation functions are found to decay exponentially and the short correlation length ξ will extend to a few sites, as shown in Fig. 9(a). Note that the ground-state properties of integer spin chains are in stark contrast to those of half-odd integer spin. In comparison, the ground state of spin-1/2 Kitaev chain

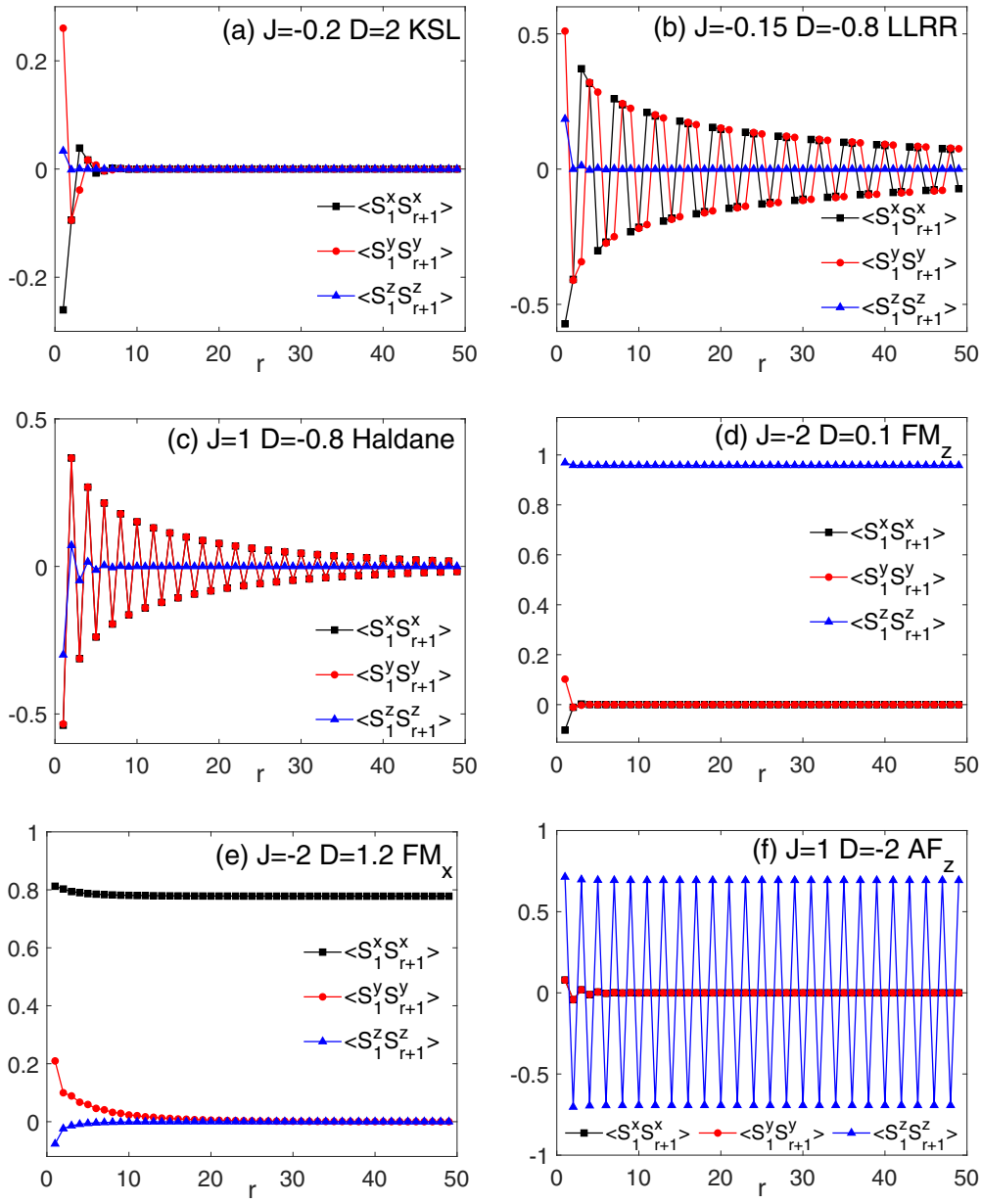

FIG. 9. The correlation between site 1 and site j with $\theta = 0$ for increasing distance $r \equiv |j-1|$ for representative points in (a) KSL phase with $J = -0.2$, $D = 2$; (b) LLRR phase with $J = -0.15$, $D = -0.8$; (c) Haldane phase with $J = 1$, $D = -0.8$; (d) FM$_z$ phase $J = -2$, $D = 0.1$; (e) FM$_x$ phase $J = -2$, $D = 1.2$; and (f) AFM$_z$ phase $J = 1$, $D = -2$. Here we use the iTEBD method and the bond dimension set as $\chi = 120$.

is $2^{N/2-1}$-fold degenerate [134], and the macroscopic degeneracy makes the ground state vulnerable. As such, an infinitesimal Heisenberg coupling is sufficient to lift the ground-state degeneracy and generate magnetic long-range order [135,136]. In contrast, the spin-1 chain supports a gapped KSL ground state, which can sustain a finite Heisenberg coupling. It is remarkable that the KSL phase becomes more robust against the Heisenberg interactions for large positive D. One can further observe that the size of the KSL phase enlarges with increasing positive D and becomes narrower for negative D. However, it is found that the three components of the dimer order parameter O_D are all mismatched in a fairly small region of the parameter space except for $J = 0$, as exhibited in Fig. 7(b).

A hallmark of the Haldane phase is the nonlocal string order parameter, which was introduced by den Nijs and Rommelse [130] and later refined by Tasaki [131]. Its limiting value reveals the hidden $\mathbb{Z}_2 \times \mathbb{Z}_2$ symmetry breaking:

$$O^{\alpha}_S(i,j) \equiv -\lim_{|i-j|\to\infty} C^{aa}(i,j). \tag{25}$$

This order parameter serves as a distinct feature of the Haldane phase. Figure 10(a) illustrates two-site correlations between sites 1 and 50. One observes that $C^z(1,50)$ is finite in the FM$_z$ phase, while the string order parameter $O^x_S(1,50)$ is nonvanishing in two regions, i.e., $-0.22 \lesssim J \lesssim -0.04$ and $J \gtrsim 0.03$. To distinguish the two phases, we plot the spin-spin correlations between site 1 and site $1+r$ for typical parameters in Fig. 9. One can observe in Fig. 9(b) that

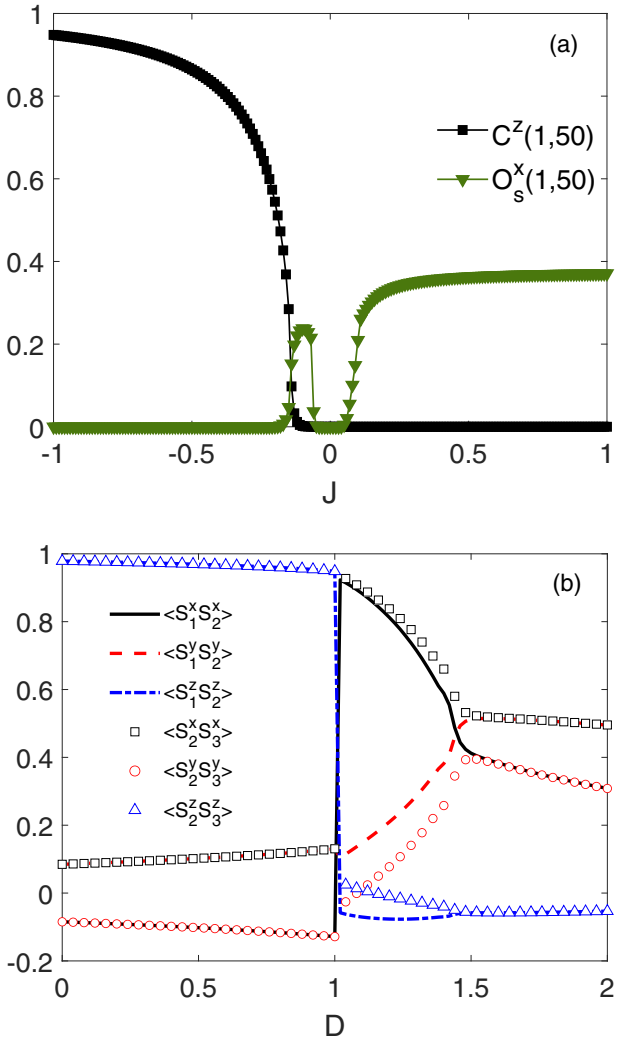

FIG. 10. (a) Two-point correlation $C^z(i, j)$ Eq. (20) with $\theta = 0$ and the string order parameter $O^x_S(i, j)$ Eq. (25) between sites 1 and 50 for $D = -0.8$ and J from -1 to 1. (b) Two-point spin-spin correlations $C^\alpha(i, j)$ Eq. (20) with $\theta = 0$ at $J = -2$. Here we use the iTEBD method and the bond dimension is set as $\chi = 120$.

both $C^x(1, 1 + r)$ and $C^y(1, 1 + r)$ alternate between two successive positive and negative values as the distance of two sites r increases, indicating the onset of the spin nematic ordering [137], while $C^x(1, 1 + r)$ and $C^y(1, 1 + r)$ decay exponentially with respect to r, manifesting the existence of the Haldane phase as demonstrated in Fig. 9(c).

Furthermore, Fig. 9(d) depicts the correlations for $J = -2$, $D = 0.1$, in which the z-component correlations $C^z(1, j)$ dominate with a value close to 1, implying the FM_z ground state, while in Fig. 9(e) the dominant correlations $C^x(1, j)$ characterize the FM_x phase for $J = -2$, $D = 1.2$. Upon increasing D at $J = -2$, the transition from FM_z to FM_x takes place at $D_c = 1$, see Fig. 10(b). Unlike the FM_z phase, the joint symmetry Eqs. (21) is broken in the FM_x phase. By further increasing the value of D, the ground state evolves from the FM_x state into the KSL phase, in which the joint symmetry is restored again. In contrast, the two-site correlation functions in Fig. 9(f) exhibit a distinct behavior. Specifically, $C^z(1, j)$ shows a periodic oscillation between values close to -1 and 1, while $C^x(1, j)$ and $C^y(1, j)$ nearly vanish. These observations provide strong evidence that the system is in the AFM_z phase.

V. SUMMARY AND CONCLUSIONS

To summarize, we have explored the physics arising from the cooperative effect of uniaxial SIA and Heisenberg interactions in the spin-1 Kitaev chain. We studied QMBS states and quantum phase transitions in spin-1 Kitaev chain with SIA. We find that the local $\mathbb{Z}_2$ gauge fields, a hallmark of the Kitaev model, are still conserved in the spin-1 Kitaev chain with SIA (KD model). In this case, the Hilbert space is fragmented into 2^N unequal subspaces characterized by $\vec{w} = \{w_1, w_n, \ldots, w_N\}$. Among an exponential number of Krylov subspaces, it has been recognized that in the uniform sector with local $\mathbb{Z}_2$ gauge fields, i.e., $\vec{w} = \{1, 1, \ldots, 1\}$, is the largest Krylov subspace, in which a local transformation maps the spin-1 KD model onto the detuned PXP model with spin-1/2 degrees of freedom, and the SIA acts as a static detuning. The dual transformation suggests a solid-state-based realization of the PXP model based on Mott insulator with strong spin-orbit and Hund's couplings.

Considering the ground states becomes twofold degenerate $|\mathbb{Z}_2\rangle$ state in the limit of $D \to -\infty$ due to the Hilbert space constraint, a continuous transition in the detuned PXP model occurs at $D_c = -0.655$. This quantum phase transition corresponds to the emergence of a dimer phase induced by the spontaneous breaking of translational symmetry in the flux-free sector which can be described by the dimer order parameter Eq. (22). We find the most prominent coherent oscillations of quantum fidelity in the quantum quench from initial states $|\mathbb{Z}_2\rangle$ and $|\mathbb{Z}_3\rangle$, a characteristic of the embedded prototypical PXP model for $D = 0$. We demonstrate that these fidelity revivals are robust against small SIA perturbation. The nonthermalizing dynamics can be also reflected by measuring the expectation values of certain local observables, which will vanish for $D < D_c$. Finally, we provide a complete phase diagram for the spin-1 KD model by describing the interplay between Kitaev interactions, Heisenberg interactions, and SIA. In particular, we underline the evolution of the Kitaev phase in a broader regime, therefore showing the relevance for the scar stability and possible solid-state applications. Seven phases are identified by the numerical methods through the corresponding spin-spin correlations, including the KSL, dimer phase, LLRR phase, Haldane phase, FM_x phase, FM_z phase, and AFM_z phase. Our study on the higher-spin Kitaev chain will likely help identify candidate materials for KSL.

ACKNOWLEDGMENTS

The authors appreciate very insightful discussions with H. Katsura, G. Sun, and Z.-X. Sun. We acknowledge M. Xue for bringing Ref. [138] to our attention. This work is supported by the National Natural Science Foundation of China (NSFC) under Grant No. 12174194, Postgraduate Research & Practice Innovation Program of Jiangsu Province under Grant No. KYCX23_0347, the National Key R&D Program of China under Grant No. 2021YFA1400803, Opening

Fund of the Key Laboratory of Aerospace Information Materials and Physics (Nanjing University of Aeronautics and Astronautics), MIIT, Top-notch Academic Programs Project of Jiangsu Higher Education Institutions (TAPP), and stable support for basic institute research under Grant No. 190101. A.M.O. kindly acknowledges Narodowe Centrum Nauki (NCN, Poland) Project No. 2021/43/B/ST3/02166 and is grateful for support via the Alexander von Humboldt Foundation Fellowship [139] (Humboldt-Forschungspreis).

APPENDIX A: MAPPING THE KITAEV MODEL WITH SINGLE-ION ANISOTROPY WITHIN FLUX-FREE SECTOR TO THE DETUNED PXP MODEL

For convenience, we use the rotated Hamiltonian Eq. (10) and set $K_j = K$. The local two-spin Hamiltonian is given by

$$\tilde{H}_{j,j+1} = KS_j^x S_{j+1}^y + D\left[\left(S_j^z\right)^2 + \left(S_{j+1}^z\right)^2\right]. \tag{A1}$$

For the five states satisfying $w_j = 1$, we have

$$\begin{aligned}
&\tilde{H}_{j,j+1}|xy\rangle = 2D|xy\rangle, \quad \tilde{H}_{j,j+1}|xz\rangle = D|xz\rangle,\\
&\tilde{H}_{j,j+1}|zy\rangle = D|zy\rangle, \quad \tilde{H}_{j,j+1}|zz\rangle = K|yx\rangle,\\
&\tilde{H}_{j,j+1}|yx\rangle = K|zz\rangle + 2D|yx\rangle.
\end{aligned} \tag{A2}$$

Accordingly, the Hamiltonian can be written in the matrix form as

$$\tilde{H}_{j,j+1} = \begin{pmatrix} 2D & 0 & 0 & 0 & 0\\ 0 & D & 0 & 0 & 0\\ 0 & 0 & D & 0 & 0\\ 0 & 0 & 0 & 2D & K\\ 0 & 0 & 0 & K & 0 \end{pmatrix}, \tag{A3}$$

which yields five energy eigenvalues $2D, D, D, D \pm \sqrt{D^2 + K^2}$. Hence, within the lowest-state manifold residing in the $w_j = 1$ sector that is spanned by $\{|zz\rangle, |yx\rangle\}$, Eq. (10) can be written for an effective model of spin-1/2 degrees of freedom, which can be simplified as

$$\hat{H}_{\mathrm{KD,eff}} = X_i + 2Dn_i. \tag{A4}$$

It is noted that the Hilbert space constraint is imposed by the projector onto the low-energy subspace spanned by configurations with no adjacent excited states, which is written as

$$\mathcal{P} = \prod_j (\mathbb{1} - n_j n_{j+1}). \tag{A5}$$

The so-called detuned PXP model Eq. (18) can be derived via the Schrieffer-Wolff transformation in the limit of strong interactions (small ϵ) of the following Hamiltonian:

$$\hat{H} = \hat{H}_0 + \epsilon \hat{H}_1. \tag{A6}$$

The leading part of Eq. (A6), $\hat{H}_0 = \sum_{j=1}^N n_j n_{j+1}$, vanishes in this subspace and we must consider the first nontrivial order that is given by $H_{\mathrm{SW}} = \epsilon \mathcal{P} H_1 \mathcal{P}$. If $\hat{H}_1$ describes the transverse field term,

$$\hat{H}_1 = \sum_{j=1}^N X_j, \tag{A7}$$

where X_j is defined in Eq. (1), we have

$$\begin{aligned}
\mathcal{P}H_1\mathcal{P} &= \prod_{i=1}^N (1 - n_i n_{i+1}) \sum_{j=1}^N X_j \prod_{k=1}^N (1 - n_k n_{k+1})\\
&= \sum_j (1 - n_{j-1}n_j)(1 - n_j n_{j+1}) X_j\\
&\quad \times (1 - n_{j-1}n_j)(1 - n_j n_{j+1})\\
&= \sum_j (X_j - n_{j-1}X_j - X_j n_{j+1} + n_{j-1}X_j n_{j+1})\\
&= \sum_j (1 - n_{j-1}) X_j (1 - n_{j+1})\\
&= \sum_j P_{j-1} X_j P_{j+1}.
\end{aligned} \tag{A8}$$

Then we consider the detuned term:

$$\hat{H}_1 = \sum_{j=1}^N n_j. \tag{A9}$$

In this case, we have

$$\begin{aligned}
\mathcal{P}H_1\mathcal{P} &= \prod_i (1 - n_i n_{i+1}) \sum_j n_j \prod_k (1 - n_k n_{k+1})\\
&= \sum_j (1 - n_{j-1}n_j)(1 - n_j n_{j+1}) n_j\\
&\quad \times (1 - n_{j-1}n_j)(1 - n_j n_{j+1})\\
&= \sum_j (n_j - n_{j-1}n_j - n_j n_{j+1} + n_{j-1}n_j n_{j+1})\\
&= \sum_j (1 - n_{j-1}) n_j (1 - n_{j+1})\\
&= \sum_j P_{j-1} n_j P_{j+1}.
\end{aligned} \tag{A10}$$

Note that a similar form can be derived even when $\hat{H}_1$ is a non-Hermitian matrix, given by

$$\hat{H}_1 = \sum_{j=1}^N iY_j, \tag{A11}$$

we also have

$$\begin{aligned}
\mathcal{P}H_1\mathcal{P} &= \prod_i (1 - n_i n_{i+1}) \sum_j (iY_j) \prod_k (1 - n_k n_{k+1})\\
&= \sum_j (1 - n_{j-1}n_j)(1 - n_j n_{j+1})(iY_j)\\
&\quad \times (1 - n_{j-1}n_j)(1 - n_j n_{j+1})\\
&= \sum_j [(iY_j) - n_{j-1}(iY_j) - (iY_j)n_{j+1} + n_{j-1}(iY_j)n_{j+1}]\\
&= \sum_j (1 - n_{j-1})(iY_j)(1 - n_{j+1})\\
&= \sum_j P_{j-1}(iY_j)P_{j+1}.
\end{aligned} \tag{A12}$$

However, if $\hat{H}_1 = \sum_{j=1}^{N} Z_j$, the PZP cannot be derived. A crucial difference is that $X_jP_j = n_jX_j$, $Y_jP_j = n_jY_j$, $n_j^2 = n_j$, while $Z_jP_j \neq n_jZ_j$.

APPENDIX B: DYNAMICAL EVOLUTION IN A QUENCH FROM INITIAL PRODUCT STATES

Here we use a similar strategy introduced for the dynamics of the generalized Hubbard models [138]. Considering a Hamiltonian $\hat{H}$ that can be separated into $\hat{H}_0$ and $\lambda\hat{V}$, where λ denotes the perturbation strength, an initial state $|\psi(0)\rangle$ evolves into $|\psi(t)\rangle = e^{-i\hat{H}t}|\psi(0)\rangle$ at any time t. If we can find an antiunitary operator $\hat{U}$ that satisfies the following conditions:

(i) $\hat{U}$ anticommutes with $\hat{H}_0$ and commutes with $\hat{V}$, i.e.,

$$\{\hat{U}, \hat{H}_0\} = 0, \quad [\hat{U}, \hat{V}] = 0. \tag{B1}$$

(ii) The initial state $|\psi(0)\rangle$ only acquires a global phase factor under $\hat{U}$, i.e.,

$$\hat{U}^{-1}|\psi(0)\rangle = e^{i\chi}|\psi(0)\rangle. \tag{B2}$$

(iii) We consider a given Hermitian operator $\hat{O}$ that is even or odd under symmetry operation by $\hat{U}$, i.e.,

$$\hat{U}^{-1}\hat{O}\hat{U} = \pm\hat{O}, \tag{B3}$$

then we can conclude

$$\langle\hat{O}\rangle_{+\lambda} = \pm\langle\hat{O}\rangle_{-\lambda}. \tag{B4}$$

Back to the KD model in Eq. (10), which can be rewritten as $\tilde{H} = \tilde{H}_{\rm K} + \hat{H}_{\rm D}$. We then apply $\hat{U} = \exp(i\pi S_j^x)$, which will yield $S_j^x \to S_j^x$, $S_j^y \to -S_j^y$, $S_j^z \to -S_j^z$. Considering condition (i), one finds

$$\hat{U}^{-1}e^{-i(\tilde{H}_{\rm K}+\hat{H}_{\rm D})t}\hat{U} = e^{-i(\tilde{H}_{\rm K}-\hat{H}_{\rm D})t}. \tag{B5}$$

To this end, in the quantum quench starting from the initial states $|\widetilde{\mathbb{Z}}_k\rangle$, e.g., $|\widetilde{\mathbb{Z}}_2\rangle$, we have

$$\begin{aligned}\langle\hat{O}\rangle_{+D} &= \langle\widetilde{\mathbb{Z}}_2|e^{i(\tilde{H}_{\rm K}+\hat{H}_{\rm D})t}\hat{O}e^{-i(\tilde{H}_{\rm K}+\hat{H}_{\rm D})t}|\widetilde{\mathbb{Z}}_2\rangle \\ &= \langle\widetilde{\mathbb{Z}}_2|Ue^{i(\tilde{H}_{\rm K}-\hat{H}_{\rm D})t}(U^{-1}\hat{O}U)e^{-i(\tilde{H}_{\rm K}-\hat{H}_{\rm D})t}U^{-1}|\widetilde{\mathbb{Z}}_2\rangle \\ &= \langle\hat{O}\rangle_{-D},\end{aligned} \tag{B6}$$

$$\begin{aligned}F(t)_{+D} &= \langle\widetilde{\mathbb{Z}}_2|e^{-i(\tilde{H}_{\rm K}+\hat{H}_{\rm D})t}|\widetilde{\mathbb{Z}}_2\rangle \\ &= \langle\widetilde{\mathbb{Z}}_2|Ue^{-i(\tilde{H}_{\rm K}-\hat{H}_{\rm D})t}U^{-1}|\widetilde{\mathbb{Z}}_2\rangle = F(t)_{-D},\end{aligned} \tag{B7}$$

where the following simple relations:

$$\begin{aligned}\hat{U}^{-1}|\widetilde{\mathbb{Z}}_2\rangle &= |x(-y)\cdots x(-y)\rangle = (-1)^{N/2}|xy\cdots xy\rangle, \\ \langle\widetilde{\mathbb{Z}}_2|\hat{U} &= \langle x(-y)\cdots x(-y)| = (-1)^{N/2}\langle xy\cdots xy|\end{aligned}$$

are used. Therefore, the values of $\langle\hat{O}\rangle$ and $F(t)$ are symmetric between positive and negative D in the quantum quench starting from the $|\widetilde{\mathbb{Z}}_2\rangle$ state. It is straightforward to generalize the theorem to other initial product states $|\widetilde{\mathbb{Z}}_k\rangle$ $(k \neq 2)$.

[1] A. Polkovnikov, K. Sengupta, A. Silva, and M. Vengalattore, Colloquium: Nonequilibrium dynamics of closed interacting quantum systems, Rev. Mod. Phys. **83**, 863 (2011).

[2] J. M. Deutsch, Quantum statistical mechanics in a closed system, Phys. Rev. A **43**, 2046 (1991).

[3] M. Srednicki, Chaos and quantum thermalization, Phys. Rev. E **50**, 888 (1994).

[4] M. Rigol, V. Dunjko, and M. Olshanii, Thermalization and its mechanism for generic isolated quantum systems, Nature (London) **452**, 854 (2008).

[5] M. Rigol and M. Srednicki, Alternatives to Eigenstate Thermalization, Phys. Rev. Lett. **108**, 110601 (2012).

[6] H. Kim, T. N. Ikeda, and D. A. Huse, Testing whether all eigenstates obey the eigenstate thermalization hypothesis, Phys. Rev. E **90**, 052105 (2014).

[7] J. M. Deutsch, Eigenstate thermalization hypothesis, Rep. Prog. Phys. **81**, 082001 (2018).

[8] P. W. Anderson, Absence of diffusion in certain random lattices, Phys. Rev. **109**, 1492 (1958).

[9] M. Rigol, V. Dunjko, V. Yurovsky, and M. Olshanii, Relaxation in a Completely Integrable Many-Body Quantum System: An ab initio Study of the Dynamics of the Highly Excited States of 1D Lattice Hard-Core Bosons, Phys. Rev. Lett. **98**, 050405 (2007).

[10] G. Biroli, C. Kollath, and A. M. Läuchli, Effect of rare Fluctuations on the Thermalization of Isolated Quantum Systems, Phys. Rev. Lett. **105**, 250401 (2010).

[11] S. Palzer, C. Zipkes, C. Sias, and M. Köhl, Quantum Transport through a Tonks-Girardeau Gas, Phys. Rev. Lett. **103**, 150601 (2009).

[12] O. Gamayun, O. Lychkovskiy, and V. Cheianov, Kinetic theory for a mobile impurity in a degenerate Tonks-Girardeau gas, Phys. Rev. E **90**, 032132 (2014).

[13] L. Barnett and A. K. Seth, Granger causality for state-space models, Phys. Rev. E **91**, 040101(R) (2015).

[14] L. Vidmar and M. Rigol, Generalized Gibbs ensemble in integrable lattice models, J. Stat. Mech.: Theory Exp. (2016) 064007.

[15] I. V. Gornyi, A. D. Mirlin, and D. G. Polyakov, Interacting Electrons in Disordered Wires: Anderson Localization and Low-T transport, Phys. Rev. Lett. **95**, 206603 (2005).

[16] D. Basko, I. Aleiner, and B. Altshuler, Metal-insulator transition in a weakly interacting many-electron system with localized single-particle states, Ann. Phys. **321**, 1126 (2006).

[17] A. Pal and D. A. Huse, Many-body localization phase transition, Phys. Rev. B **82**, 174411 (2010).

[18] A. Lazarides, A. Das, and R. Moessner, Fate of Many-Body Localization Under Periodic Driving, Phys. Rev. Lett. **115**, 030402 (2015).

[19] E. Altman, Many-body localization and quantum thermalization, Nat. Phys. **14**, 979 (2018).

[20] M. Schreiber, S. S. Hodgman, P. Bordia, H. P. Lüschen, M. H. Fischer, R. Vosk, E. Altman, U. Schneider, and I. Bloch, Observation of many-body localization of interacting fermions in a quasirandom optical lattice, Science **349**, 842 (2015).

[21] K. Pakrouski, P. N. Pallegar, F. K. Popov, and I. R. Klebanov, Many-Body Scars as a Group Invariant Sector of Hilbert Space, Phys. Rev. Lett. **125**, 230602 (2020).

[22] M. Rigol, Breakdown of Thermalization in Finite one-Dimensional Systems, Phys. Rev. Lett. **103**, 100403 (2009).

[23] D. A. Abanin, E. Altman, I. Bloch, and M. Serbyn, Colloquium: Many-body localization, thermalization, and entanglement, Rev. Mod. Phys. **91**, 021001 (2019).

[24] H. Bernien, S. Schwartz, A. Keesling, H. Levine, A. Omran, H. Pichler, S. Choi, A. S. Zibrov, M. Endres, M. Greiner, V. Vuletić, and M. D. Lukin, Probing many-body dynamics on a 51-atom quantum simulator, Nature (London) **551**, 579 (2017).

[25] S. Choi, C. J. Turner, H. Pichler, W. W. Ho, A. A. Michailidis, Z. Papić, M. Serbyn, M. D. Lukin, and D. A. Abanin, Emergent SU(2) Dynamics and Perfect Quantum Many-Body Scars, Phys. Rev. Lett. **122**, 220603 (2019).

[26] T. Iadecola, M. Schecter, and S. Xu, Quantum many-body scars from magnon condensation, Phys. Rev. B **100**, 184312 (2019).

[27] C.-J. Lin, V. Calvera, and T. H. Hsieh, Quantum many-body scar states in two-dimensional Rydberg atom arrays, Phys. Rev. B **101**, 220304(R) (2020).

[28] T. Iadecola and M. Schecter, Quantum many-body scar states with emergent kinetic constraints and finite-entanglement revivals, Phys. Rev. B **101**, 024306 (2020).

[29] K. Bull, J.-Y. Desaules, and Z. Papić, Quantum scars as embeddings of weakly broken Lie algebra representations, Phys. Rev. B **101**, 165139 (2020).

[30] C. J. Turner, J.-Y. Desaules, K. Bull, and Z. Papić, Correspondence Principle for Many-Body Scars in Ultracold Rydberg Atoms, Phys. Rev. X **11**, 021021 (2021).

[31] M. Ljubotina, B. Roos, D. A. Abanin, and M. Serbyn, Optimal steering of matrix product states and quantum many-body scars, PRX Quantum **3**, 030343 (2022).

[32] B. Windt and H. Pichler, Squeezing Quantum Many-Body Scars, Phys. Rev. Lett. **128**, 090606 (2022).

[33] J. Ren, C. Liang, and C. Fang, Deformed symmetry structures and quantum many-body scar subspaces, Phys. Rev. Res. **4**, 013155 (2022).

[34] S. Dooley, S. Pappalardi, and J. Goold, Entanglement enhanced metrology with quantum many-body scars, Phys. Rev. B **107**, 035123 (2023).

[35] P. Zhang, H. Dong, Y. Gao, L. Zhao, J. Hao, J.-Y. Desaules, Q. Guo, J. Chen, J. Deng, B. Liu, W. Ren, Y. Yao, X. Zhang, S. Xu, K. Wang, F. Jin, X. Zhu, B. Zhang, H. Li, C. Song *et al.*, Many-body Hilbert space scarring on a superconducting processor, Nat. Phys. **19**, 120 (2023).

[36] S. D. Geraedts, R. Nandkishore, and N. Regnault, Many-body localization and thermalization: Insights from the entanglement spectrum, Phys. Rev. B **93**, 174202 (2016).

[37] W. W. Ho, S. Choi, H. Pichler, and M. D. Lukin, Periodic Orbits, Entanglement, and Quantum many-body Scars in Constrained Models: Matrix Product State Approach, Phys. Rev. Lett. **122**, 040603 (2019).

[38] S. Moudgalya, B. A. Bernevig, and N. Regnault, Quantum many-body scars and Hilbert space fragmentation: A review of exact results, Rep. Prog. Phys. **85**, 086501 (2022).

[39] Z.-X. Gong and L.-M. Duan, Prethermalization and dynamic phase transition in an isolated trapped ion spin chain, New J. Phys. **15**, 113051 (2013).

[40] B. Neyenhuis, J. Zhang, P. W. Hess, J. Smith, A. C. Lee, P. Richerme, Z.-X. Gong, A. V. Gorshkov, and C. Monroe, Observation of prethermalization in long-range interacting spin chains, Sci. Adv. **3**, e1700672 (2017).

[41] Y. Tang, W. Kao, K.-Y. Li, S. Seo, K. Mallayya, M. Rigol, S. Gopalakrishnan, and B. L. Lev, Thermalization Near Integrability in a Dipolar Quantum Newton's Cradle, Phys. Rev. X **8**, 021030 (2018).

[42] W. Kao, K.-Y. Li, K.-Y. Lin, S. Gopalakrishnan, and B. L. Lev, Topological pumping of a 1D dipolar gas into strongly correlated prethermal states, Science **371**, 296 (2021).

[43] T. Kinoshita, T. Wenger, and D. S. Weiss, A quantum Newton's cradle, Nature (London) **440**, 900 (2006).

[44] K. Xu, J.-J. Chen, Y. Zeng, Y.-R. Zhang, C. Song, W. Liu, Q. Guo, P. Zhang, D. Xu, H. Deng, K. Huang, H. Wang, X. Zhu, D. Zheng, and H. Fan, Emulating Many-Body Localization with a Superconducting Quantum Processor, Phys. Rev. Lett. **120**, 050507 (2018).

[45] Q. Guo, C. Cheng, Z.-H. Sun, Z. Song, H. Li, Z. Wang, W. Ren, H. Dong, D. Zheng, Y.-R. Zhang, R. Mondaini, H. Fan, and H. Wang, Observation of energy-resolved many-body localization, Nat. Phys. **17**, 234 (2021).

[46] J. Ren, C. Liang, and C. Fang, Quasisymmetry Groups and Many-Body Scar Dynamics, Phys. Rev. Lett. **126**, 120604 (2021).

[47] I. Affleck, T. Kennedy, E. H. Lieb, and H. Tasaki, Rigorous Results on Valence-Bond Ground States in Antiferromagnets, Phys. Rev. Lett. **59**, 799 (1987).

[48] S. Moudgalya, N. Regnault, and B. A. Bernevig, Entanglement of exact excited states of Affleck-Kennedy-Lieb-Tasaki models: Exact results, many-body scars, and violation of the strong eigenstate thermalization hypothesis, Phys. Rev. B **98**, 235156 (2018).

[49] M. Schecter and T. Iadecola, Weak Ergodicity Breaking and Quantum Many-Body Scars in Spin-1 XY magnets, Phys. Rev. Lett. **123**, 147201 (2019).

[50] J.-Y. Desaules, A. Hudomal, C. J. Turner, and Z. Papić, Proposal for Realizing Quantum Scars in the Tilted 1D Fermi-Hubbard Model, Phys. Rev. Lett. **126**, 210601 (2021).

[51] D. Jaksch, J. I. Cirac, P. Zoller, S. L. Rolston, R. Côté, and M. D. Lukin, Fast Quantum Gates Neutral Atoms, Phys. Rev. Lett. **85**, 2208 (2000).

[52] C. J. Turner, A. A. Michailidis, D. A. Abanin, M. Serbyn, and Z. Papić, Weak ergodicity breaking from quantum many-body scars, Nat. Phys. **14**, 745 (2018).

[53] V. Khemani, C. R. Laumann, and A. Chandran, Signatures of integrability in the dynamics of Rydberg-blockaded chains, Phys. Rev. B **99**, 161101(R) (2019).

[54] C.-J. Lin and O. I. Motrunich, Exact Quantum Many-Body scar States in the Rydberg-Blockaded Atom Chain, Phys. Rev. Lett. **122**, 173401 (2019).

[55] D. K. Mark, C.-J. Lin, and O. I. Motrunich, Exact eigenstates in the Lesanovsky model, proximity to integrability and the PXP model, and approximate scar states, Phys. Rev. B **101**, 094308 (2020).

[56] B. Mukherjee, S. Nandy, A. Sen, D. Sen, and K. Sengupta, Collapse and revival of quantum many-body scars via Floquet engineering, Phys. Rev. B **101**, 245107 (2020).

[57] M. Serbyn, D. A. Abanin, and Z. Papić, Quantum many-body scars and weak breaking of ergodicity, Nat. Phys. **17**, 675 (2021).

[58] G. Roux, Finite-size effects in global quantum quenches: Examples from free bosons in an harmonic trap and the one-dimensional Bose-Hubbard model, Phys. Rev. A **81**, 053604 (2010).

[59] P. Sierant and J. Zakrzewski, Many-body localization of bosons in optical lattices, New J. Phys. **20**, 043032 (2018).

[60] H. Zhao, J. Vovrosh, F. Mintert, and J. Knolle, Quantum Many-Body Scars in Optical Lattices, Phys. Rev. Lett. **124**, 160604 (2020).

[61] B. Mukherjee, A. Sen, D. Sen, and K. Sengupta, Restoring coherence via aperiodic drives in a many-body quantum system, Phys. Rev. B **102**, 014301 (2020).

[62] J. C. Halimeh, I. P. McCulloch, B. Yang, and P. Hauke, Tuning the topological θ-angle in cold-atom quantum simulators of gauge theories, PRX Quantum **3**, 040316 (2022).

[63] P. Fendley, K. Sengupta, and S. Sachdev, Competing density-wave orders in a one-dimensional hard-boson model, Phys. Rev. B **69**, 075106 (2004).

[64] S. Trebst, M. Troyer, Z. Wang, and A. W. W. Ludwig, A short introduction to Fibonacci anyon models, Prog. Theor. Phys. Suppl. **176**, 384 (2008).

[65] I. Lesanovsky and H. Katsura, Interacting Fibonacci anyons in a Rydberg gas, Phys. Rev. A **86**, 041601(R) (2012).

[66] A. Chandran, F. J. Burnell, and S. L. Sondhi, Absence of Fibonacci anyons in Rydberg chains, Phys. Rev. B **101**, 075104 (2020).

[67] R. Moessner and S. L. Sondhi, Ising models of quantum frustration, Phys. Rev. B **63**, 224401 (2001).

[68] C. R. Laumann, R. Moessner, A. Scardicchio, and S. L. Sondhi, Quantum Adiabatic Algorithm and Scaling of Gaps at First-Order Quantum Phase Transitions, Phys. Rev. Lett. **109**, 030502 (2012).

[69] F. M. Surace, P. P. Mazza, G. Giudici, A. Lerose, A. Gambassi, and M. Dalmonte, Lattice Gauge Theories and String Dynamics in Rydberg Atom Quantum Simulators, Phys. Rev. X **10**, 021041 (2020).

[70] I. Chi Chen and T. Iadecola, Emergent symmetries and slow quantum dynamics in a Rydberg-atom chain with confinement, Phys. Rev. B **103**, 214304 (2021).

[71] J.-Y. Desaules, D. Banerjee, A. Hudomal, Z. Papić, A. Sen, and J. C. Halimeh, Weak ergodicity breaking in the Schwinger model, Phys. Rev. B **107**, L201105 (2023).

[72] J.-Y. Desaules, A. Hudomal, D. Banerjee, A. Sen, Z. Papić, and J. C. Halimeh, Prominent quantum many-body scars in a truncated Schwinger model, Phys. Rev. B **107**, 205112 (2023).

[73] P. Sala, T. Rakovszky, R. Verresen, M. Knap, and F. Pollmann, Ergodicity Breaking Arising from Hilbert Spacefragmentation in Dipole-Conserving Hamiltonians, Phys. Rev. X **10**, 011047 (2020).

[74] S. Moudgalya, N. Regnault, and B. A. Bernevig, η-pairing in Hubbard models: From spectrum generating algebras to quantum many-body scars, Phys. Rev. B **102**, 085140 (2020).

[75] K. Mizuta, K. Takasan, and N. Kawakami, Exact Floquet quantum many-body scars under Rydberg blockade, Phys. Rev. Res. **2**, 033284 (2020).

[76] B. Mukherjee, Z. Cai, and W. V. Liu, Constraint-induced breaking and restoration of ergodicity in spin-1 PXP models, Phys. Rev. Res. **3**, 033201 (2021).

[77] A. A. Michailidis, C. J. Turner, Z. Papić, D. A. Abanin, and M. Serbyn, Stabilizing two-dimensional quantum scars by deformation and synchronization, Phys. Rev. Res. **2**, 022065(R) (2020).

[78] C. J. Turner, A. A. Michailidis, D. A. Abanin, M. Serbyn, and Z. Papić, Quantum scarred eigenstates in a Rydberg atom chain: Entanglement, breakdown of thermalization, and stability to perturbations, Phys. Rev. B **98**, 155134 (2018).

[79] G.-X. Su, H. Sun, A. Hudomal, J.-Y. Desaules, Z.-Y. Zhou, B. Yang, J. C. Halimeh, Z.-S. Yuan, Z. Papić, and J.-W. Pan, Observation of many-body scarring in a Bose-Hubbard quantum simulator, Phys. Rev. Res. **5**, 023010 (2023).

[80] Z. Yao, L. Pan, S. Liu, and H. Zhai, Quantum many-body scars and quantum criticality, Phys. Rev. B **105**, 125123 (2022).

[81] C. Peng and X. Cui, Bridging quantum many-body scars and quantum integrability in Ising chains with transverse and longitudinal fields, Phys. Rev. B **106**, 214311 (2022).

[82] W.-L. You, G. Sun, J. Ren, W. C. Yu, and A. M. Oleś, Quantum phase transitions in the spin-1 Kitaev-Heisenberg chain, Phys. Rev. B **102**, 144437 (2020).

[83] W.-L. You, Z. Zhao, J. Ren, G. Sun, L. Li, and A. M. Oleś, Quantum many-body scars in spin-1 Kitaev chains, Phys. Rev. Res. **4**, 013103 (2022).

[84] A. Kitaev, Anyons in an exactly solved model and beyond, Ann. Phys. **321**, 2 (2006).

[85] G. Jackeli and G. Khaliullin, Mott Insulators in the Strong Spin-Orbit Coupling Limit: From Heisenberg to a Quantum Compass and Kitaev Models, Phys. Rev. Lett. **102**, 017205 (2009).

[86] H. Liu, J. Chaloupka, and G. Khaliullin, Kitaev Spin Liquid in 3*d* Transition Metal Compounds, Phys. Rev. Lett. **125**, 047201 (2020).

[87] Y. Li, G. Chen, W. Tong, L. Pi, J. Liu, Z. Yang, X. Wang, and Q. Zhang, Rare-Earth Triangular Lattice Spin Liquid: A Single-Crystal Study of $YbMgGaO_4$, Phys. Rev. Lett. **115**, 167203 (2015).

[88] W. Ruan, Y. Chen, S. Tang, J. Hwang, H.-Z. Tsai, R. L. Lee, M. Wu, H. Ryu, S. Kahn, F. Liou, C. Jia, A. Aikawa, C. Hwang, F. Wang, Y. Choi, S. G. Louie, P. A. Lee, Z.-X. Shen, S.-K. Mo, and M. F. Crommie, Evidence for quantum spin liquid behaviour in single-layer 1T-$TaSe_2$ from scanning tunnelling microscopy, Nat. Phys. **17**, 1154 (2021).

[89] J. Wu, J. Li, Z. Zhang, C. Liu, Y. H. Gao, E. Feng, G. Deng, Q. Ren, Z. Wang, R. Chen, J. Embs, F. Zhu, Q. Huang, Z. Xiang, L. Chen, Y. Wu, E. S. Choi, Z. Qu, L. Li, J. Wang *et al.*, Magnetic field effects on the quantum spin liquid behaviors of $NaYbS_2$, Quantum Front. **1**, 13 (2022).

[90] P. Khuntia, M. Velazquez, Q. Barthélemy, F. Bert, E. Kermarrec, A. Legros, B. Bernu, L. Messio, A. Zorko, and P. Mendels, Gapless ground state in the archetypal quantum kagome antiferromagnet $ZnCu_3(OH)_6Cl_2$, Nat. Phys. **16**, 469 (2020).

[91] A. C. Shockley, F. Bert, J.-C. Orain, Y. Okamoto, and P. Mendels, Frozen State and Spin Liquid Physics in $Na_4Ir_3O_8$: An NMR Study, Phys. Rev. Lett. **115**, 047201 (2015).

[92] A. Banerjee, J. Yan, J. Knolle, C. A. Bridges, M. B. Stone, M. D. Lumsden, D. G. Mandrus, D. A. Tennant, R. Moessner, and S. E. Nagler, Neutron scattering in the proximate quantum spin liquid α-$RuCl_3$, Science **356**, 1055 (2017).

[93] R. Yadav, R. Ray, M. S. Eldeeb, S. Nishimoto, L. Hozoi, and J. van den Brink, Strong Effect of Hydrogen Order on Magnetic Kitaev Interactions in $H_3LiIr_2O_6$, Phys. Rev. Lett. **121**, 197203 (2018).

[94] S. Pal, A. Seth, P. Sakrikar, A. Ali, S. Bhattacharjee, D. V. S. Muthu, Y. Singh, and A. K. Sood, Probing signatures of fractionalization in the candidate quantum spin liquid Cu_2IrO_3 via anomalous Raman scattering, Phys. Rev. B **104**, 184420 (2021).

[95] Y. Imai, K. Nawa, Y. Shimizu, W. Yamada, H. Fujihara, T. Aoyama, R. Takahashi, D. Okuyama, T. Ohashi, M. Hagihala, S. Torii, D. Morikawa, M. Terauchi, T. Kawamata, M. Kato, H. Gotou, M. Itoh, T. J. Sato, and K. Ohgushi, Zigzag magnetic order in the Kitaev spin-liquid candidate material $RuBr_3$ with a honeycomb lattice, Phys. Rev. B **105**, L041112 (2022).

[96] T. Halloran, F. Desrochers, E. Z. Zhang, T. Chen, L. E. Chern, Z. Xu, B. Winn, M. Graves-Brook, M. B. Stone, A. I. Kolesnikov, Y. Qiu, R. Zhong, R. Cava, Y. B. Kim, and C. Broholm, Geometrical frustration versus Kitaev interactions in $BaCo_2(AsO_4)_2$, Proc. Natl. Acad. Sci. **120**, e2215509119 (2023).

[97] B. Gao, T. Chen, D. W. Tam, C.-L. Huang, K. Sasmal, D. T. Adroja, F. Ye, H. Cao, G. Sala, M. B. Stone, C. Baines, J. A. T. Verezhak, H. Hu, J.-H. Chung, X. Xu, S.-W. Cheong, M. Nallaiyan, S. Spagna, M. B. Maple, A. H. Nevidomskyy *et al.*, Experimental signatures of a three-dimensional quantum spin liquid in effective spin-1/2 $Ce_2Zr_2O_7$ pyrochlore, Nat. Phys. **15**, 1052 (2019).

[98] L. E. Chern, Y. B. Kim, and C. Castelnovo, Competing quantum spin liquids, gauge fluctuations, and anisotropic interactions in a breathing pyrochlore lattice, Phys. Rev. B **106**, 134402 (2022).

[99] P. P. Stavropoulos, D. Pereira, and H.-Y. Kee, Microscopic Mechanism for a Higher-Spin Kitaev Model, Phys. Rev. Lett. **123**, 037203 (2019).

[100] A. Koga, H. Tomishige, and J. Nasu, Ground-state and thermodynamic properties of an $S = 1$ Kitaev model, J. Phys. Soc. Jpn. **87**, 063703 (2018).

[101] H.-Y. Lee, N. Kawashima, and Y. B. Kim, Tensor network wave function of $S = 1$ Kitaev spin liquids, Phys. Rev. Res. **2**, 033318 (2020).

[102] Y.-H. Chen, J. Genzor, Y. B. Kim, and Y.-J. Kao, Excitation spectrum of spin-1 Kitaev spin liquids, Phys. Rev. B **105**, L060403 (2022).

[103] R. Pohle, N. Shannon, and Y. Motome, Spin nematics meet spin liquids: Exotic quantum phases in the spin-1 bilinear-biquadratic model with Kitaev interactions, Phys. Rev. B **107**, L140403 (2023).

[104] K. M. Taddei, V. O. Garlea, A. M. Samarakoon, L. D. Sanjeewa, J. Xing, T. W. Heitmann, C. dela Cruz, A. S. Sefat, and D. Parker, Zigzag magnetic order and possible Kitaev interactions in the spin-1 honeycomb lattice $KNiAsO_4$, Phys. Rev. Res. **5**, 013022 (2023).

[105] S. Mohapatra and A. C. Balram, Pronounced quantum many-body scars in the one-dimensional spin-1 Kitaev model, Phys. Rev. B **107**, 235121 (2023).

[106] C. Xu, J. Feng, M. Kawamura, Y. Yamaji, Y. Nahas, S. Prokhorenko, Y. Qi, H. Xiang, and L. Bellaiche, Possible Kitaevquantum Spin Liquid State in 2D Materials with $S = 3/2$, Phys. Rev. Lett. **124**, 087205 (2020).

[107] H.-K. Jin, W. M. H. Natori, F. Pollmann, and J. Knolle, Unveiling the $S = 3/2$ Kitaev honeycomb spin liquids, Nat. Commun. **13**, 3813 (2022).

[108] W. M. H. Natori, H.-K. Jin, and J. Knolle, Quantum liquids of the $S = 3/2$ Kitaev honeycomb and related Kugel-Khomskii models, Phys. Rev. B **108**, 075111 (2023).

[109] K. Fukui, Y. Kato, J. Nasu, and Y. Motome, Ground-state phase diagram of spin-S Kitaev-Heisenberg models, Phys. Rev. B **106**, 174416 (2022).

[110] C. Xu, J. Feng, H. Xiang, and L. Bellaiche, Interplay between Kitaev interaction and single ion anisotropy in ferromagnetic CrI_3 and $CrGeTe_3$ monolayers, npj Comput. Mater. **4**, 57 (2018).

[111] O. Bradley and R. R. P. Singh, Instabilities of spin-1 Kitaev spin liquid phase in presence of single-ion anisotropies, Phys. Rev. B **105**, L060405 (2022).

[112] E. S. Sørensen, J. Riddell, and H.-Y. Kee, Islands of chiral solitons in integer-spin Kitaev chains, Phys. Rev. Res. **5**, 013210 (2023).

[113] R. S. Fishman, Single-ion anisotropy is necessary and appropriate to study the magnetic behavior of Tb^{3+} moments with $J_{\text{eff}} = \frac{1}{2}$ on the honeycomb lattice in $Tb_2Ir_3Ga_9$, Phys. Rev. B **103**, 214440 (2021).

[114] M. P. Zaletel, R. S. K. Mong, C. Karrasch, J. E. Moore, and F. Pollmann, Time-evolving a matrix product state with long-ranged interactions, Phys. Rev. B **91**, 165112 (2015).

[115] M. Fishman, S. R. White, and E. M. Stoudenmire, The ITensor Software Library for Tensor Network Calculations, SciPost Phys. Codebases 4 (2022).

[116] G. Vidal, Classical Simulation of Infinite-Size Quantum Lattice Systems in one Spatial Dimension, Phys. Rev. Lett. **98**, 070201 (2007).

[117] D. Sen, R. Shankar, D. Dhar, and K. Ramola, Spin-1 Kitaev model in one dimension, Phys. Rev. B **82**, 195435 (2010).

[118] Y. Sugita, Y. Kato, and Y. Motome, Antiferromagnetic Kitaev interactions in polar spin-orbit Mott insulators, Phys. Rev. B **101**, 100410(R) (2020).

[119] J. A. Sears, L. E. Chern, S. Kim, P. J. Bereciartua, S. Francoual, Y. B. Kim, and Y.-J. Kim, Ferromagnetic Kitaev interaction and the origin of large magnetic anisotropy in α-$RuCl_3$, Nat. Phys. **16**, 837 (2020).

[120] S. Moudgalya, B. A. Bernevig, and N. Regnault, Quantum many-body scars in a Landau level on a thin torus, Phys. Rev. B **102**, 195150 (2020).

[121] A. Daniel, A. Hallam, J.-Y. Desaules, A. Hudomal, G.-X. Su, J. C. Halimeh, and Z. Papić, Bridging quantum criticality via many-body scarring, Phys. Rev. B **107**, 235108 (2023).

[122] The data and the code that support the findings of this study are available from the corresponding authors upon reasonable request.

[123] T. M. R. Byrnes, P. Sriganesh, R. J. Bursill, and C. J. Hamer, Density matrix renormalization group approach to the massive Schwinger model, Phys. Rev. D **66**, 013002 (2002).

[124] E. Rico, T. Pichler, M. Dalmonte, P. Zoller, and S. Montangero, Tensor Networks for Lattice Gauge Theories and Atomic Quantum Simulation, Phys. Rev. Lett. **112**, 201601 (2014).

[125] B. Yang, H. Sun, R. Ott, H.-Y. Wang, T. V. Zache, J. C. Halimeh, Z.-S. Yuan, P. Hauke, and J.-W. Pan, Observation of gauge invariance in a 71-site Bose–Hubbard quantum simulator, Nature **587**, 392 (2020).

[126] M. V. Damme, J. C. Halimeh, and P. Hauke, Gauge-symmetry violation quantum phase transition in lattice gauge theories, arXiv:2010.07338.

[127] C.-J. Lin, A. Chandran, and O. I. Motrunich, Slow thermalization of exact quantum many-body scar states under perturbations, Phys. Rev. Res. **2**, 033044 (2020).

[128] C. M. Langlett, Z.-C. Yang, J. Wildeboer, A. V. Gorshkov, T. Iadecola, and S. Xu, Rainbow scars: From area to volume law, Phys. Rev. B **105**, L060301 (2022).

[129] L. Gotta, S. Moudgalya, and L. Mazza, Asymptotic quantum many-body scars, arXiv:2303.05407.

[130] M. den Nijs and K. Rommelse, Preroughening transitions in crystal surfaces and valence-bond phases in quantum spin chains, Phys. Rev. B **40**, 4709 (1989).

[131] H. Tasaki, Quantum Liquid in Antiferromagnetic Chains: A Stochastic Geometric Approach to the Haldane Gap, Phys. Rev. Lett. **66**, 798 (1991).

[132] G.-H. Liu, L.-J. Kong, and W.-L. You, Quantum phase transitions in spin-1 compass chains, Eur. Phys. J. B **88**, 284 (2015).

[133] S. M. Winter, A. A. Tsirlin, M. Daghofer, J. van den Brink, Y. Singh, P. Gegenwart, and R. Valentí, Models and materials for generalized Kitaev magnetism, J. Phys.: Condens. Matter **29**, 493002 (2017).

[134] W.-L. You and G.-S. Tian, Quantum phase transition in the one-dimensional compass model using the pseudospin approach, Phys. Rev. B **78**, 184406 (2008).

[135] F. Trousselet, A. M. Oleś, and P. Horsch, Compass-Heisenberg model on the square lattice—spin order and elementary excitations, Europhys. Lett. **91**, 40005 (2010).

[136] F. Trousselet, A. M. Oleś, and P. Horsch, Magnetic properties of nanoscale compass-Heisenberg planar clusters, Phys. Rev. B **86**, 134412 (2012).

[137] A. A. Zvyagin, V. V. Slavin, and G. A. Zvyagina, Manifestation of spin nematic ordering in the spin-1 chain system, Phys. Rev. B **107**, 134421 (2023).

[138] J. Yu, N. Sun, and H. Zhai, Symmetry Protected Dynamical Symmetry in the Generalized Hubbard Models, Phys. Rev. Lett. **119**, 225302 (2017).

[139] Alexander von Humboldt Foundation Forschungspreis.